HARMONIA CA21119

Deliverable 1.3

Harmonised AOD retrievals & AOD comparisons

Authors: Lionel Doppler[1], Angelos Karanikolas[2], Meritxell Garcia Suñer[3], Gaurav Kumar[3], Stelios Kazadzis[2], Natalia Kouremeti[2]

Date: 27 October 2026

[1] Meteorologisches Observatorium Lindenberg - Richard-Aßmann-Observatorium, Deutscher Wetterdienst (MOL-RAO, DWD), Lindenberg (Tauche), Germany

[2] Physikalisch-Meteorologisches Observatorium Davos / World Radiation Center (PMOD/WRC), Davos, Switzerland

[3] Facultat de Física, Universitat de València Estudi General (UVEG), Burjassot (Valencia), Spain

Table of Content

Table of Content ... 2

1. Introduction ... 3

2. Harmonised AOD comparison ... 5

2.1 Method ... 8

2.1.1 Definition of (AOD_{harm}) the harmonised AOD retrieved from TOD ... 8

2.1.2 Process to obtain (AOD_{harm}) out of the information delivered by the networks and compare it to each other ... 9

2.1.3. Selection of fixed SZA values for monitoring over long time series or for comparisons of different stations ... 9

2.2 Prede/PFR/CIMEL intercomparison on Lindenberg Dataset ... 10

2.2.1 Lindenberg instrument suite, Lindenberg Dataset and dataset used in this study ... 11

2.2.2 (AOD_{harm}) comparison at fixed SZA ... 12

2.2.4 Influence of the age of the calibration ... 17

2.3 PFR/CIMEL intercomparisons on GAW-PFR stations ... 18

2.3.1 Preparation of the dataset and quality analysis ... 20

2.3.2 Harmonised AOD comparison (AOD_{harm}) CIMEL minus PFR in dependence of the airmass. Statistics and analyses ... 23

2.3.3 Evolution of the difference of harmonised AOD (AOD_{harm}) CIMEL minus PFR on a long time series ... 27

2.4 Summary of the AOD comparison on the harmonised AOD dataset ... 29

3. Harmonisation and comparison experiments during FRC-VI campaign ... 30

3.1 FRC-V and FRC-VI campaigns ... 30

3.1.1. FRC (Filter Radiometer Comparisons) campaigns in Davos ... 30

3.1.2. Introduction to the FRC-VI (Sixth WMO Filter Radiometer Comparison) ... 31

3.2 Outcomes from the FRC-VI campaign: harmonisation of AOD measurements from Prede and CIMEL instruments ... 32

3.2.1. The Sunrad algorithm ... 33

3.2.2. Instrumentation ... 33

3.2.3. Measurement days ... 33

3.2.4. Assessing the differences between AERONET and SKYNET networks using the Sunrad algorithm. ... 34

3.2.5. Conclusions 46
3.2.6. Outlook 46
4. Harmonisation for lunar photometry: Moonrad (SKYNET algorithm for lunar photometry) 46
4.1. Moonrad implementation and structure 47
4.1.1 Moonrad 47
4.1.2. ROLO module 47
4.1.3. DSFORM and DSPROC 47
4.2. Comparison to CIMEL lunar AOD 48
4.2.1. Dataset 48
4.2.2. Intercomparison with AERONET 48
4.2.3. Future work 52
5. Summary 52
References 53
Table of Acronyms 57
Acknowledgements 59

1. Introduction

The primary objective of COST Action HARMONIA is to enhance measurement and retrieval methods in aerosol remote sensing. A key parameter characterizing aerosols is the **Aerosol Optical Depth (AOD)**. The photometry technique involves retrieving AOD using remote-sensing methods based on measurements of solar irradiance at specific wavelengths. These measurements account for the attenuation of radiation as it passes through the atmosphere, as described by the Beer–Lambert-Bouguer law (equation (E2.1)). By combining direct solar irradiance measurements with this law, the total optical depth (TOD) is obtained. The term "total" refers to the sum of contributions from all atmospheric constituents to the optical depth. The AOD is then derived as the aerosol contribution to the TOD. The instruments used for these irradiance measurements include filter radiometers (also known as "photometers") and spectroradiometers.

In deliverable D1.2 (Doppler et al. 2024) of HARMONIA's Working Group 1, we presented diverse methods of AOD retrieval and quantified the impact of various methods and instrumentations on the obtained AOD values. The present deliverable, along with deliverable D1.4 (Karanikolas et al. 2026), builds upon the findings of Deliverable D1.2: Deliverable D1.4 focuses on the retrieval of AOD at higher spectral resolution (using spectroradiometers) and also AOD retrievals in the UV (ultraviolet) and IR (infrared). The present deliverable, however, is focused on AOD retrievals using traditional photometers (filter radiometers) that employ filters to measure irradiance and derive AOD for a reduced number of spectral channels (ranging from four to eight, depending on

the instrument type). Here we present the newest studies conducted during the second half of the HARMONIA COST Action (October 2024 - October 2026) and we propose a method to harmonise the AOD dataset of measurements taken with traditional instruments: CIMEL (networks AERONET and CÆLIS), Prede POM & POM02 (network SKYNET), and PFR (Precision Filter Radiometer, network GAW-PFR).

There have been various comparisons between the instrument networks, mostly through short-term campaigns, but in certain cases over longer time periods too. Deliverable D1.1 (Doppler et al., 2023) includes a long list of short-term campaigns and comparisons. On the Island of Tenerife, at Izaña - AEMET site IARC (Izaña Atmospheric Research Center), AOD of AERONET (CIMEL instruments) and GAW-PFR are measuring in parallel for more than 20 years. Cuevas et al. (2019) compared the AOD over a twelve-year period and attempted to explain the causes for differences outside the WMO limits. Therefore, they investigated to what extent various factors such as post processing differences, different field of view and time difference between the measurements of each instrument of up to 30 seconds can create large AOD differences. Karanikolas et al. (2022) compared the AOD between AERONET and GAW-PFR over a 13 years period in Davos-Switzerland and investigated the consistency of long-term trends between the networks under different methodologies and temporal resolution differences. Nakajima et al. (2020) presented AOD comparisons at 870 nm between SKYNET and GAW-PFR or AERONET during short-term campaigns in different locations (Davos, Valencia, Rome, Tokyo, Pune and Seoul). Karanikolas et al. (2024) compared AOD from GAW-PFR, AERONET and SKYNET over three campaigns in Davos and three in Rome, the longest being several months long. They also recalibrated participating Prede POM instruments using PFR instruments as reference and recalculated its AOD with the same algorithm and different calibration. As a result, they were able to show the pure effect of different calibration approaches on AOD and the remaining AOD differences originating from post processing differences. Karanikolas et al. (2025) included AOD comparisons between AERONET and GAW-PFR in 4 locations (Davos, Izaña, Hohenpeißenberg and Lindenberg) from the start of parallel measurements until 2022. Deliverable 1.2 (Doppler et al., 2024) includes comparisons between AERONET, GAW-PFR and SKYNET instruments in Lindenberg for the entire time series of each pair of parallel measurements.

Most of the aforementioned studies, including the various campaigns in deliverable D1.1, concern AOD comparisons of the original AOD provided by each network separately and therefore the differences include all factors affecting AOD (calibration and post processing differences, instrument technical characteristics, cloud screening, operation protocols etc.). The exceptions were Cuevas et al. (2019) and Karanikolas et al. (2024) as we mentioned. These 2 studies had a different focus, locations and instruments. Both studies provided indication of the effect of post processing AOD (particularly Cuevas et al., 2019), but a full comparison of AOD for the same instrument and calibration with different post processing under different conditions or the comparison of various instruments with harmonised post processing was not in their scope. Post processing over the 3 networks being a secondary objective in those 2 studies, not part of the main focus. Part of this deliverable (mainly part 2) focuses on this matter with intention to fill that gap and demonstrate the effect of using a harmonised AOD retrieval method in comparison to the procedures of each network, under different conditions and in different locations.

This deliverable also builds upon the very first deliverable of Working Group 1: D1.1 (Doppler et al. 2023), which presented the AOD measurement campaigns aimed at cross-comparisons, quality evaluation, and improvements. Therefore, part 3 presents the activities of a very important campaign that occurred after the publication of D1.1: The Sixth Filter Radiometer Comparison (FRC-VI) of September and October 2025. FRC campaigns are organized by the World Meteorological Organisation (WMO) and are scheduled every five years at PMOD/WRC (the World radiation centre) in Davos, Switzerland. Part 3 describes the campaign itself and a unique harmonisation study conducted during FRC-VI: the application of the SKYNET network's AOD retrieval algorithm "Sunrad" to the raw irradiance measurements of the CIMEL photometer, which is the instrument used by the AERONET network. Finally, part 4 presents the new outcomes of the lunar extension of the SKYNET network: the development and validation of the lunar AOD algorithm "Moonrad," enabling Prede-POM02 photometers of the SKYNET network to perform AOD measurements not only during the day with solar irradiance but also during the night with lunar irradiance retrievals.

2. Harmonised AOD comparison

We first recapitulate the process of AOD retrieval.
We consider the Beer-Lambert-Bouguer law (equation (E2.1)) describing the attenuation of irradiance I at a given wavelength (λ) or a given spectral channel:

$$I = I_0 e^{-m\tau} \quad \text{(E2.1)}$$

where (I) is the direct solar irradiance on the ground at a particular wavelength, (I_0) the direct solar irradiance at the top of the atmosphere at the same wavelength (extraterrestrial irradiance), (m) the optical air mass coefficient (a general approximation of the airmass is the geometric optical airmass: m = m_{geom} = 1/cos(SZA) with SZA is the Solar Zenith Angle) and (τ) the total optical depth (TOD) of the atmosphere. (TOD) is the sum of all individual optical depths of each atmospheric component (gases and aerosols, absorption and scattering).

We can express Beer-Lambert-Bouguer law in a logarithm form replacing (τ) with (TOD):

$$TOD = [\ln(I_0) - \ln(I)] / m \quad \text{(E2.2)}$$

Equation (E2.2) demonstrates that if we know the extraterrestrial irradiance (I_0), and measure the irradiance (I) with the filter radiometer, and calculate the airmass (m), then we can consequently retrieve the total optical depth (TOD).

There are two methods for estimating the ratio (I/I_0):

- The first method involves precisely measuring the absolute value of the irradiance (I) with a well-calibrated radiometer and using the very precise tabulated value of the extraterrestrial irradiance (I_0). This approach is used for AOD retrieval from spectroradiometer measurements, which is the topic of deliverable D1.4 (Karanikolas et al., 2026).
- The second method used for photometers (filter radiometers) does not require measuring the absolute value of the irradiance (I) in $W.m^{-2}$. Instead, it is sufficient to have a stable instrument and take the raw signal of the radiation measurement (we

name it (V), since the raw signal is typically a voltage), provided that the relative value of the solar radiation that the instrument would measure if placed at the top of the atmosphere is known. This hypothetical extraterrestrial raw signal is denoted as (V_0).

Focusing on this second method, Equation (E2.2) is now:

$$TOD = [\ln(V_0) - \ln(V)] / m \quad \text{(E2.3)}$$

The challenge is to determine (V_0). This is achieved using the calibration method “Langley Plot”, a method inherited from astronomy research. If the atmosphere is stable and the Total Optical Depth (TOD) is low and does not change significantly (conditions typically met in a dry atmosphere with minimal aerosols, such as tops of mountains distant from pollution sources), (V) measurements are taken during sunrise. As the sun's elevation increases, the Solar Zenith Angle (SZA) decreases, and the airmass (m) increases. We plot the evolution of (ln(V)) as a function of (m). If the TOD remains constant, the resulting graph is a straight line that decreases with increasing (m), with a slope equal to the value of (TOD). By extrapolating this line to (m = 0), we obtain the value of ($\ln(V_0)$).

The challenging aspect of photometry is obtaining a valid value of (V_0) for the instrument. This involves conducting regular and robust calibrations while ensuring the stability of the instruments, as (V_0) should not change significantly over a period of 3-5 years. A typical schedule for instrument calibrations is every 1.5-2 years.

The estimation of (V_0) — which encompasses the quality of the calibration, the stability of the instrument, and the regularity of the calibration schedule — determines the difference in Total Optical Depth (TOD) and, consequently, in Aerosol Optical Depth (AOD) measured by two different systems.

To quantify these differences (and thus estimate the quality of a system and improve it), it is essential to eliminate certain artificial discrepancies arising from the retrieval method itself. These discrepancies occur during the computation of Aerosol Optical Depth (AOD) from Total Optical Depth (TOD). Each network (e.g., AERONET, CÆLIS, SKYNET, GAW-PFR) employs its own method for this computation. Let us examine the equation relating (TOD) and (AOD) to better understand this process. For the spectral channels that we consider in this study (λ = 500 nm and λ = 870 nm) we consider that only ozone (O_3) and NO_2 are absorbing the radiation. Equation (E2.4) is a simple expression of it:

$$TOD = AOD + OD_{Ray} + OD_{O3} + OD_{NO2} \quad \text{(E2.4)}$$

With:

- (TOD) Total Optical Depth
- (AOD) Aerosol Optical Depth
- (OD_{Ray}) Rayleigh Optical Depth: Optical Depth due to molecular scattering of all air molecules of the atmosphere
- (OD_{O3}) Optical Depth due to ozone (O_3) absorption of radiation
- (OD_{NO2}) Optical Depth due to nitrogen dioxide (NO_2) absorption of radiation

Unfortunately in reality, it is much more complicated and the airmass “m” is not simply the geometrical airmass ($m = m_{geom} = 1/\cos(SZA)$), but because of refraction due to the curvature of the atmosphere, each term in Equation (E2.4) has its own airmass, which depends on the mean (or barycentric) altitude of the atmospheric component associated with each term. We obtain therefore Equation (E2.5):

$$m_{TOD} \times TOD = m_{Aer} \times AOD + m_{Ray} \times OD_{Ray} + m_{O3} \times OD_{O3} + m_{No2} \times OD_{NO2} \quad \text{(E2.5)}$$

(OD_{Ray}), (OD_{O3}), (OD_{NO2}) are computed as following:

$$OD_{Ray} = CoeffRay(\lambda) \times P$$

$$OD_{O3} = CoeffO3(\lambda) \times O3DU \quad \text{(E2.5a)}$$

$$OD_{NO2} = CoeffNO2(\lambda) \times NO2DU$$

- With CoeffRay(λ): A wavelength (λ) dependent coefficient obtained from a more complex formulation of atmospheric molecular scattering that is derived from Rayleigh theory. In most cases, this coefficient is a simplified version of the formulation presented by Bodhaine et al. (1999).
- With CoeffO3(λ): A wavelength (λ) dependent coefficient characterizing the ozone absorption of radiation over the spectral channel centered on the wavelength (λ).
- With CoeffNO2(λ): A wavelength (λ) dependent coefficient characterizing the NO_2 absorption of radiation over the spectral channel centered on the wavelength (λ).
- P: The atmospheric pressure at the measurement station in mbar (milibar).
- O3DU: The Total Ozone Column (TOC) over the measurement station in Dobson Units (DU)
- NO2DU: The Total NO_2 Column over the measurement station in Dobson Units (DU)

Integrating these parameters to equation (E2.5), we can formulate TOD like this:

$$TOD = (m_{aer} \times AOD + m_{Ray} \times CoeffRay(\lambda) \times P + m_{O3} \times CoeffO3(\lambda) \times O3DU + m_{No2} \times CoeffNO2(\lambda) \times NO2DU) / m_{TOD} \quad \text{(E2.6)}$$

And we can formulate AOD like this:

$$AOD = (m_{TOD} \times TOD - m_{Ray} \times CoeffRay(\lambda) \times P - m_{O3} \times CoeffO3(\lambda) \times O3DU - m_{No2} \times CoeffNO2(\lambda) \times NO2DU) / m_{aer} \quad \text{(E2.7)}$$

Equation (E2.7) involves in addition to TOD (obtained with radiation measurement, Beer-Lambert-Bouguer and calibration information) 11 coefficients or parameters:

- Five airmasses coefficients (m_{aer}, m_{TOD}, m_{Ray}, m_{o3}, m_{NO2})

- Three coefficients of molecular scattering or gas absorption (CoeffRay(λ), CoeffO3(λ), CoeffNO2(λ))
- Three quantities of atmospheric components (P, O3DU, NO2DU)

The challenge of AOD comparisons between instruments of different networks is that these 11 coefficients or parameters are defined or obtained differently. The definition of them are explained in following reference papers or manuals:

- For AERONET, ($AOD_{AERONET}$) in Giles et al. (2019)
- For CÆLIS, (AOD_{CAELIS}) in González et al. (2020)
- For GAW-PFR, (AOD_{PFR}) in Wehrli (2009)
- For SKYNET, (AOD_{SKYNET}) in Nakajima et al. (2020)

The method applied in this part of the deliverable (part 2., here and later in section 2.2 for the comparison Prede - CIMEL - PFR on Lindenberg Dataset as in 2.3 for the comparison CIMEL-PFR on four GAW-PFR stations) is to define an harmonised AOD: (AOD_{harm}), and compute (AOD_{harm}) for all instruments and then compare the (AOD_{harm}) obtained for CIMEL, Prede or PFR to each other's.

This method is presented in the following section (2.1).

2.1 Method

2.1.1 Definition of (AOD_{harm}) the harmonised AOD retrieved from TOD

We decided to align (AOD_{harm}) with (AOD_{PFR}), following GAW-PFR network criteria (Wehrli, 2009), namely:

- $m_{TOD} = m_{Ray} = m_{RKY}$ of Kasten and Young (1989)
- CoeffNO2(λ) = 0 for the considered wavelength (λ = 500 and 862 or 870 nm)
- CoeffNO2(λ) = 0.031E-3 DU^{-1} (for λ = 500 nm) & 0.002E-3 DU^{-1} (for λ = 862 nm) from Gueymard (1995) tabulated values.
- CoeffRay(λ) = $\delta_{RFS}(\lambda)$ of Fröhlich and Shaw (1980)
- (m_{O3}) is from Komhyr (1989) considering Ozone layer height (h = 22km), station altitude (r) in km (r = altitude above sea level) and Earth radius (R) in km (R = 6370 km).
- (m_{aer}) is the airmass (m_a) from Kasten (1966), a slightly decreased version of geometric airmass especially for high solar elevations.

(AOD_{harm}) is therefore formulated following:

$$\mathbf{AOD_{harm} = AOD_{PFR} = TOD - (m_{RKY} \times \delta_{RFS}(\lambda) \times P - m_{O3} \times CoeffO3(\lambda) \times O3DU - m_{No2} \times CoeffNO2(\lambda) \times NO2DU) / m_{aer}} \quad \textbf{(E2.8)}$$

For atmospheric components' amount, we usually obtain pressure (P) and total ozone column (O3DU) with 1-min measured pressure at the station and daily Total Ozone Column.

2.1.2 Process to obtain (AOD_{harm}) out of the information delivered by the networks and compare it to each other

Usually, the networks of photometers (AERONET, CÆLIS, SKYNET, GAW-PFR) deliver AOD values (AOD_{netw}: $AOD_{AERONET}$, AOD_{CAELIS}, AOD_{SKYNET}, and AOD_{PFR} respectively) following their own rules for the diverse terms and parameters of equation (E2.7), and inform the amount of atmospheric components used for the calculation (air pressure, ozone and sometimes NO_2).

The process has three steps:

1) **STEP 1: Reconstruction of (TOD) out of (AOD_{netw})**

For all networks we apply equation (E2.6) with the amount of atmospheric parameters informed by the network and using the networks' coefficients as detailed above (after equation (E2.7)) and calculate back the total optical depth (TOD).

Note, that for the networks AERONET and CÆLIS, the TOD is delivered by the network itself, it is therefore not necessary to reconstruct (TOD) from (AOD_{netw}) using (E2.6).

2) **STEP 2: Computation of harmonised AOD (AOD_{harm})**

We define the common pressure, ozone dataset for the comparison and from the TOD obtained for each instrument/network at step (1) and apply equation (E2.8) and the parameters of PFR computation defined in subsection 2.1.1 above equation (E2.8) and we obtain (AOD_{harm}) for each instrument.

3) **STEP 3: Comparison of harmonised AOD of each instrument to each other**

(AOD_{harm}) of each instrument are independent from the computational method of each network and can be compared to each other.

2.1.3. Selection of fixed SZA values for monitoring over long time series or for comparisons of different stations

From Beer-Lambert-Bouguer equation (E2.1), we can define the relative error on Total Optical Depth (TOD): ($\Delta_{rel}TOD = \Delta TOD/TOD$) due to the relative error ($\Delta_{rel}(I/I_0) = \Delta(I/I_0)/(I/I_0)$) on the attenuation of radiation (I/I_0):

$$\Delta_{rel}TOD = \Delta_{rel}(I/I_0) / m \qquad \text{(E2.9)}$$

With (m) the airmass, approximately: m = 1/cos(SZA)

(E2.9) means that, the higher is the sun elevation, the lower is the solar zenith angle (SZA) and the lower is the airmass (m) and the higher is the error on TOD, and consequently, the higher is the error on AOD.

In summary: **The higher is the sun, the higher is the error on AOD and the less precise is the photometry technique.**

This is the reason why, the World Meteorological Organisation (WMO) defines for AOD comparison criteria of limit of acceptance ($WMO_{tolerance}$) that are decreasing with airmass (m):

$$WMO_{tolerance} = 0.005 + 0.01 / m \qquad \text{(E2.10)}$$

With m, the airmass, usually the geometric airmass: $m = m_{geom} = 1/\cos(SZA)$

This property—the fact that the accuracy of photometry and optical-depth retrieval depends on the solar zenith angle (SZA)—leads to fallacies of thinking:

1) When stations situated at of low latitudes (eg Izaña that is below 30°N) are compared to stations situated at higher latitudes (eg. Hohenpeißenberg that is over 47°N) since the SZA during the day in Izaña is up to 17° lower than in Hohenpeißenberg, the airmass is in Izaña in average much lower than in Hohenpeißenberg and therefore the condition for a precise photometry worse. Consequently, the difference in AOD is greater on average over time. This does not mean that the atmospheric conditions of the site (weather: Clouds or pollution) are worth, or that the instruments are worth.

2) When we make the instrumental comparison at the same station, during a longer time series (eg one complete year), since in spring and summer the solar elevation is higher, the SZA lower and the airmass consequently also lower, the AOD differences between different systems are consequently higher on average over time in summer/spring than in autumn/winter. This does not mean that there are better conditions (temperature, weather, pollution) for measurements in winter than in summer or that the instruments are getting worse in summer.

A solution to make an objective comparison between different stations or over long time series over different seasons on a same station is to consider not a daily or long time average of the AOD difference, but to select a fixed SZA value for these comparison studies. In the studies presented in this document we will consider SZA = 70°. It is a low solar elevation but it has the advantage that this SZA value is reached also for the stations situated over 45° of latitude (Lindenberg, Hohenpeißenber, Davos) even in winter.

2.2 Prede/PFR/CIMEL intercomparison on Lindenberg Dataset

In HARMONIA Deliverable D1.2 (Doppler et al., 2024), in subsection 3.1.2, we have already presented two intercomparison studies between Prede, PFR and CIMEL photometers leaded by Angelos Karanikolas (PMOD/WRC) and Pablo González Sicilia (AEMET/IARC) using the Lindenberg Dataset. These comparisons were comparison of (AOD_{netw}): The original AOD as provided by the networks (SKYNET for Prede, AERONET for CIMEL and from the GAW-PFR algorithm of DWD -version v2.25, 2009, for PFR).
Here we continue these studies using the harmonised AOD as defined in previous section (2.1): The parameter (AOD_{harm}) as defined in equation (E2.8) in subsection 2.1.1 in order to get rid of the differences due to the different methods that the different networks use to compute (AOD) out of total optical depth (TOD) respecting equation (E2.7).
In addition, for comparison of AOD of different systems over long time series, we consider the method of selecting only values of a fixed SZA. This method and its necessity is explained in subsection 2.1.3.

2.2.1 Lindenberg instrument suite, Lindenberg Dataset and dataset used in this study

The Observatory Lindenberg MOL-RAO (Meteorologisches Observatorium Lindenberg - Richard-Aßmann-Observatorium) of the German meteorological service “Deutscher Wetterdienst” (DWD) is the only station worldwide that has Prede, PFR and CIMEL AOD measurements in parallel during a time series.
DWD Lindenberg (MOL-RAO) is a 70 staff member observatory that is a supersite for meteorology, atmospheric component and atmospheric physical processes (eg. radiation) measurements. It was founded in 1905 by Richard Aßmann, one of the fathers of aerology and balloon carried meteorological measurements.
MOL-RAO is situated in a rural zone, for Germany a clean air and background station, in the flat lands of the region Brandenburg, in the North-East of Germany, 65 km air line South-East of the city of Berlin. Lindenberg is a village (Ort) part of the commune (Gemeinde) Tauche. The geocoordinates of DWD Lindenberg are (14.12 E, 52.21 N, 121 m).
DWD Lindenberg instrumental suite for AOD measurements with photometers is presented in Figure 2.2.1 with information about the systems, the networks to which each instrument belongs and date information about since when the systems are making continuous measurements and since when the current dataset is available for the station Lindenberg.



Figure 2.2.1 The current AOD instrumental suite of DWD Lindenberg: CIMEL, Prede and PFR, with detailed information: Picture and complete instrument denomination (2nd row from

top), named of the network to which each instruments belongs (third row) and (lowest row) year from which measurements began (in brackets the year from which data of the current dataset are available).

We concretely used following dataset for this study in Lindenberg:

- For PFR instruments: Network is almost GAW-PFR; it is a DWD-owned processed dataset with an algorithm taken from GAW-PFR algorithm version 2.25 of 2009. We take the product named "Level 3" in GAW-PFR data level architecture which is similar to an AERONET or CÆLIS Level 1.5 data level or a SKYNET Level 2A data level; Data available are 2016 - 2022 for verified quality data that we decided to process for this study.
- For Prede instruments: The SKYNET dataset Level 2 disponible on SKYNET-ISDC (International SKYNET Data Center): https://www.skynet-isdc.org/ for the station Lindenberg, Method "ESR-Sunrad", Version "v0.9-1", Level L2.; Data available: 2016-2022
- For CIMEL Instruments:
    - AERONET data Level 2 disponible on AERONET website: https://aeronet.gsfc.nasa.gov/, Collection "AEROSOL OPTICAL DEPTH (V3)-SOLAR", Station "MetObs_Lindenberg", Data available: 2013 - 2025
    - CÆLIS data Level 1.5 directly obtained from GOA-UVa (University of Valladolid / Group of Atmospheric Optics). Data available: 2013 - 2026. In contrary of AERONET, CÆLIS provides data for both instruments running in parallel: CIMEL #919 and CIMEL #787.

For all these datasets we made the three steps procedure explained in subsection 2.1.2:

1) Step 1: Retrieve TOD from the AOD (when necessary = only for SKYNET dataset)
2) Step 2: We computed (AOD_{harm}) with respect to equation (E2.8) for each instrument type, and for CIMEL instruments. For CIMEL instruments we did it as well for AERONET as original dataset and for CÆLIS as original dataset. For CÆLIS, even for both CIMEL instruments running in parallel: CIMEL #919 and CIMEL #787
3) Step3: We computed (AOD_{harm}) differences between the different systems.

After this, since we want to analyse the time evolution over 10 years of the (AOD_{harm}) differences, we reduced the (AOD_{harm}) differences datasets to the SZA values of SZA = 70° only (the reason why we did this is explained in subsection 2.1.3.

2.2.2 (AOD_{harm}) comparison at fixed SZA

We reduced the Lindeberg Dataset selecting only the AOD comparisons for SZA = 70°. We can therefore make an objective analysis of the evolution of the differences in (AOD_{harm}) for each pair of instrument type (CIMEL, Prede and PFR) during the time. This is shown in figure 2.2:

- ($AOD_{harm\text{-}CIMEL}$) minus ($AOD_{harm\text{-}PFR}$) is in blue squares on the picture
- ($AOD_{harm\text{-}PFR}$) minus ($AOD_{harm\text{-}Prede}$) is in green triangles on the picture
- ($AOD_{harm\text{-}Prede}$) minus ($AOD_{harm\text{-}CIMEL}$) is in red circles on the picture

For this study ($AOD_{harm\text{-}CIMEL}$) is taken from the AERONET level 2.0 dataset and ($AOD_{harm\text{-}Prede}$) is taken from the SKYNET level 2.0 dataset.

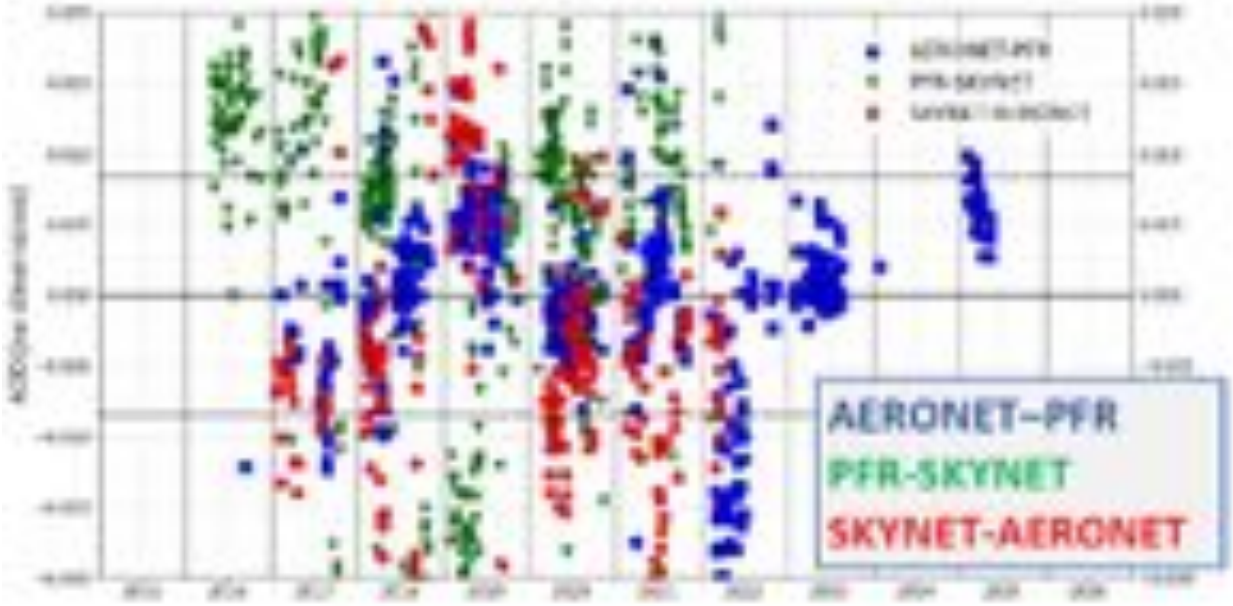


Figure 2.2.2 (AOD_{harm}) comparison in dependence of time for the measurements at a fixed SZA value of 70° only. ($AOD_{harm\text{-}CIMEL}$ - $AOD_{harm\text{-}PFR}$) in blue squares, ($AOD_{harm\text{-}PFR}$ - $AOD_{harm\text{-}Prede}$) in green triangles, ($AOD_{harm\text{-}Prede}$ - $AOD_{harm\text{-}CIMEL}$) in red circles.

Figure 2.2.2 shows a good agreement between ($AOD_{harm\text{-}CIMEL}$) and ($AOD_{harm\text{-}PFR}$) (blue squares) , which is confirmed statistically in the table of figure 2.2.3. With some exceptions like during the year 2022, the difference ($AOD_{harm\text{-}CIMEL}$) minus ($AOD_{harm\text{-}PFR}$) is most of the time inside of the WMO limits. On the other hand, figure 2.2 shows that Prede instrument does not match that much to PFR and CIMEL (comparisons to PFR in green triangles and comparison to CIMEL in red circles): Only about the half of the (AOD_{harm}) differences are inside the WMO limits. This is confirmed statistically in the table of figure 2.2.4. The reason why is, that SKYNET calibration procedure of the Prede instrument differs from PFR and CIMEL ones: PFR and CIMEL instruments go to the GAW-PFR GAW-PFR centre (the World Optical Depth Research and Calibration Center -WORCC) or to an AERONET calibration centre (PHOTONS at the laboratory of atmospheric optics - LOA- of University of Lille or the group of atmospheric optics - GOA - at University of Valladolid) and there they become the calibration transferred from a reference instrument having been calibrated with the Langley Plot method on a mountain (Izaña in Tenerife or Mauna Loa in Hawaii for the CIMEL instruments). The Prede instruments, on another hand, are calibrated on the site of the measurements with an improved Langley Plot method that allows the Langley Plot calibration also at sites that are not that suited to Langley Plot calibrations than mountains like Izaña or Mauna Loa. The advantage of the SKYNET procedure is that the instrument does not need to travel, consequently there are no travel damages and there are no breaks in the measurement dataset. The inconvenience is that it is challenging to make a Langley Plot calibration onsite and the process can be complicated and need some post-processing improvements. Therefore ($AOD_{harm\text{-}Prede}$) differs from the (AOD_{harm})

of CIMEL and PFR. But thanks to the connections and networking of COST action HARMONIA, there is enough exchanges and feedback between the SKYNET European responsible people and the staff of the main Prede stations in Europe (incl. DWD Lindenberg) and the improvement of the quality of the Prede calibration and dataset is in process. The improved results will be shown in outlook studies.

Figure 2.2.3 shows the differences between the harmonised AOD out of the CÆLIS dataset (Level 1.5) and out of the AERONET dataset for both CIMEL instruments (#919 in cyan triangles and #787 in light blue triangles). There is a difference between (AOD_{harm}) between the data taken originally from AERONET and from CÆLIS, because between CÆLIS and AERONET it is not only a different method of data processing as detailed in E2.7 (AERONET and CÆLIS AOD computing out of TOD are very indeed very similar) but CÆLIS and AERONET datasets involved in this study use different calibration values V_0, since CÆLIS dataset used here is a Level 1.5 dataset and AERONET dataset used here is a Level 2 dataset (explanation below after the figure 2.2.3).
Figure 2.2.3 shows also thanks to CÆLIS Dataset that provides data for both CIMEL instruments working in parallel (#919 and #787) the differences of (AOD_{harm}) between each CIMEL instrument and the PFR: ($AOD_{harm\text{-}CIMEL919}$ - $AOD_{harm\text{-}PFR}$) in orange squares and ($AOD_{harm\text{-}CIMEL787}$ - $AOD_{harm\text{-}PFR}$) in magenta squares. The graphic of the figure 2.2.3 does not reveal a large difference between the AOD difference distribution of CIMEL#919 vs PFR and of CIMEL#787 vs PFR. To show in detail which CIMEL instrument matches better to PFR, we need to look at the table of figure 2.2.4 with the statistics value, and we see that #919 slightly better matches (lower values of mean bias and mean absolute bias).

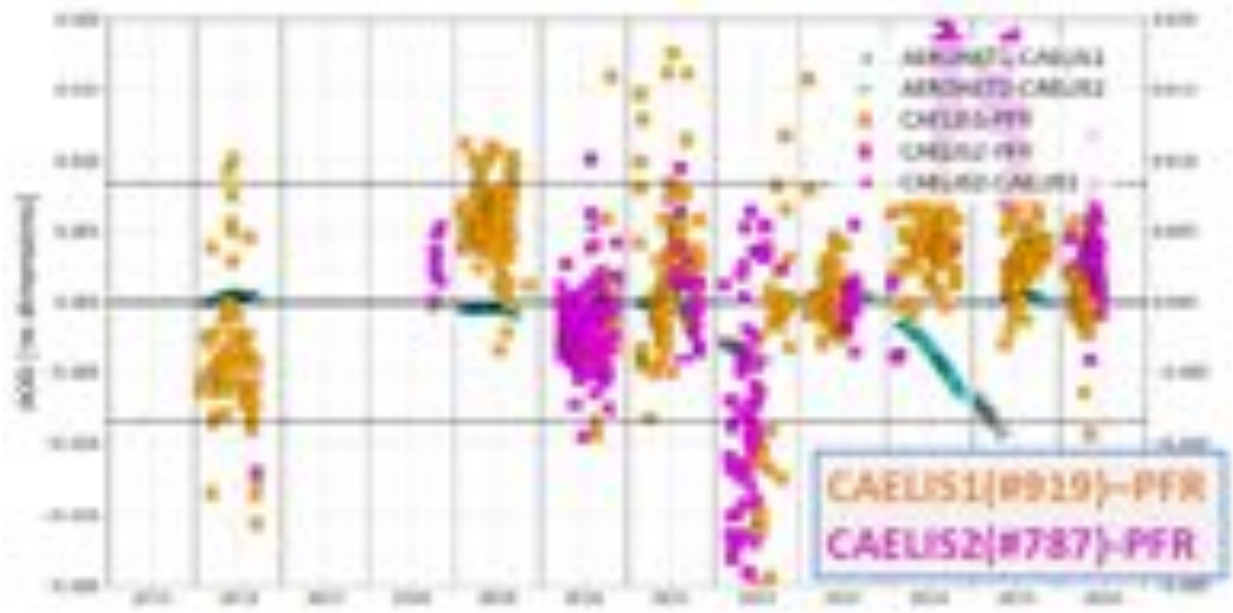


Figure 2.2.3 (AOD_{harm}) comparison in dependence of time for the measurements at a fixed SZA value of 70° only. ($AOD_{harm\text{-}AERONET}$ - $AOD_{harm\text{-}CAELIS}$) in cyan triangles for CIMEL #919 and in light blue triangles for CIMEL #787; ($AOD_{harm\text{-}CIMEL919}$ - $AOD_{harm\text{-}PFR}$) with CIMEL taken from CÆLIS in

orange squares and ($AOD_{harm\text{-}CIMEL787}$ - $AOD_{harm\text{-}PFR}$) with CIMEL taken from CÆLIS in magenta squares.

Figure 2.2.3 demonstrates one weakness of our study: AERONET Level 2.0 is compared to CÆLIS Level 1.5 for both instruments (cyan and light blue triangles on Figure 2.2.3). AERONET Level 2.0 uses calibration values V_0 (see equation (E2.3) and before) based on the interpolation in days between the last calibration and the next calibration (AERONET Level 2 product is therefore only available for the dates before the last realised calibration); when CÆLIS Level 1.5 product uses the calibration values V_0 from the last calibration. Therefore, AERONET Level 2.0 calibration values evolve from day to day and CÆLIS Level 1.5 values evolve in steps of about 1,5 to 2 years (time between two calibrations of the CIMEL instrument). The consequence on the AOD difference is therefore visible: these are the drifts of the cyan and hell blue triangles moving from - 0.001 to -0.0010 in 2024 and 2025 on Figure 2.2.3.
An outlook (already in process in collaboration with colleagues of University of Valladolid), is to develop a CÆLIS Level 2 product using the same definition of calibration values V_0 as AERONET do for its Level 2.0 product. This study will be then updated with comparisons AERONET Level 1.5 vs CÆLIS Level 1.5 and AERONET Level 2 vs CÆLIS Level 2.

Figure 2.2.4 summarizes the performances of all (AOD_{harm}) comparisons for SZA = 70°.
In the first column, there are listed all the comparisons done:

- CIMEL (A) - PFR is ($AOD_{harm\text{-}CIMEL}$ - $AOD_{harm\text{-}PFR}$) for CIMEL data taken from AERONET Level 2.0 dataset
- CIMEL_919 (C) - PFR is ($AOD_{harm\text{-}CIMEL919}$ - $AOD_{harm\text{-}PFR}$) for CIMEL instrument serial #919 data taken from CÆLIS Level 1.5 dataset
- CIMEL_787 (C) - PFR is ($AOD_{harm\text{-}CIMEL787}$ - $AOD_{harm\text{-}PFR}$) for CIMEL instrument serial #787 data taken from CÆLIS Level 1.5 dataset
- PREDE (S) - PFR is ($AOD_{harm\text{-}Prede}$ - $AOD_{harm\text{-}PFR}$) for Prede data taken from SKYNET Level 2.0 dataset
- CIMEL_787 (C) - CIMEL_919 (C) is ($AOD_{harm\text{-}CIMEL787}$ - $AOD_{harm\text{-}CIMEL919}$) for CIMEL instrument serial #787 vs CIMEL instrument serial #919 data taken from CÆLIS Level 1.5 dataset

The second column gives the number of days with measurements at SZA=70° that are available in the Lindenberg Dataset for each instrument pair that are compared to each other in this study.
The two last columns are the statistics. Mean(BE70) is the average of the bias on the AOD differences for all the SZA 70° comparisons. More relevant for a quality analysis is the mean of the absolute value of the AOD difference: Mean(abs(BE70)) in the last column.



	n_days	Mean(BE70)	Mean(abs(BE70))
CIMEL (AERONET) – PFR	870	+0.00005	0.0059
CIMEL_919 (CAELIS) – PFR	615	+0.00242	0.0070
CIMEL_787 (CAELIS) – PFR	401	+0.00534	0.0160
PREDE (SKYNET) – PFR	470	+0.00073	0.0189
CIMEL_787 (CAELIS) – CIMEL_919 (CAELIS)	166	+0.00299	0.0101

WMO acceptance criterion: Bias (SZA=70°) <= 0.0085

Figure 2.2.4 Table of performances. First column: Systems involved in the comparisons with serial numbers for the CIMEL data processed by CÆLIS. The original network is informed in brackets.

Last column of the table of figure 2.2.4 gives the most important value to compare the quality of the measurements: The mean of the absolute bias between (AOD_{harm}) of one instrument to the other on the whole SZA=70° dataset available (number of days with SZA 70° available are in column 2).
We notice, that the CIMEL vs PFR comparisons ($AOD_{harm\text{-}CIMEL}$ - $AOD_{harm\text{-}PFR}$) are very close to each other independently of which CIMEL instrument (#787 or #919) is involved. With a mean absolute bias < 0.006 CIMEL vs PFR comparison is definitively inside the WMO limits of acceptance (difference should be below 0.0085 at SZA=70°).

The statistics of the table of Figure 2.2.4 confirms what we observed on the graphic of figure 2.2.5 for Prede vs other instruments ($AOD_{harm\text{-}PFR}$ - $AOD_{harm\text{-}Prede}$) in green triangles and ($AOD_{harm\text{-}Prede}$ - $AOD_{harm\text{-}CIMEL}$) in red circles on the graphic of figure 2.2.2: Comparison between Prede and other instruments is mostly not completely inside WMO limits, but more at the limit (means absolute bias of column 4 of the table of figure 2.2.4 is above 0.18, more than twice the WMO criterion value). Fortunately HARMONIA gave us the opportunity to work together with SKYNET Europe responsible people (at CNR/ISAC and University of Valencia) that are part of HARMONIA and the initiated common work with them helped to improve the SKYNET dataset understanding, and make post-processings. Outlook work of this study will show better values of comparisons of ($AOD_{harm\text{-}Prede}$ - $AOD_{harm\text{-}CIMEL}$) and ($AOD_{harm\text{-}Prede}$ - $AOD_{harm\text{-}PFR}$).

CÆLIS belonging is for this study crucial, since it allows to have data of both CIMEL instruments (#919 and #787) running in parallel in Lindenberg which AERONET does not allow (only data of one instrument are available for each AERONET station). With CÆLIS dataset it was possible to compare (AOD_{harm}) of CIMEL #787 to CIMEL #919: ($AOD_{harm\text{-}CIMEL787}$ - $AOD_{harm\text{-}CIMEL919}$): Last row of the table of Figure 2.2.4. The mean absolute bias (0.010094) is almost at

the value of the WMO limit (0.0085). Nevertheless in an outlook study, it will be investigated if the statistics is not made worse because of some periods of technical issues of one instrument (probably #787 since its comparison to PFR -row 3 in the table, is worse than the comparison of #919 to PFR - row 4) or maybe even of both instruments at some periods (for example in 2022 - see figures 2.2.2 and 2.2.3) or probably more the PFR instrument since the two CIMEL instruments seem to agree with each other in this period.

2.2.4 Influence of the age of the calibration

We investigate if the age of the calibration of one system (CIMEL instrument, official AERONET calibration done during the time of this study at GOA-UVa in Valladolid), or the other (PFR instrument, calibration done at the GAW-PFR calibration centre WORCC at PMOD/WRC in Davos).
For this, we plot the (AOD_{harm}) difference CIMEL minus PFR ($AOD_{harm\text{-}CIMEL}$ - $AOD_{harm\text{-}PFR}$) in dependence of the age of the calibration of the instruments. Figure 2.2.5 shows ($AOD_{harm\text{-}CIMEL}$ - $AOD_{harm\text{-}PFR}$) in dependence of the age of the calibration of the PFR instrument.

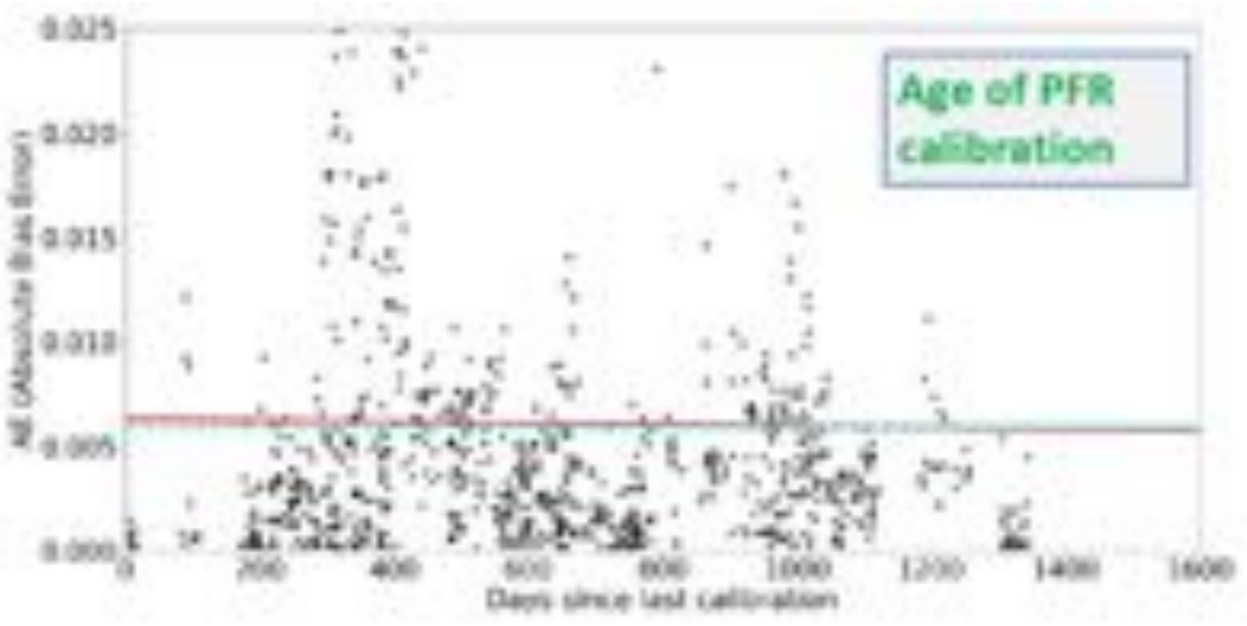


Figure 2.2.5 Absolute difference of (AOD_{harm}) CIMEL minus PFR ($AOD_{harm\text{-}CIMEL}$ - $AOD_{harm\text{-}PFR}$) in dependence of the age (in days) of the calibration of the PFR instrument. Cyan dashed line: Mean absolute bias, red plain line is a linear regression.

There is no significant trend of the differences in relation to time from last calibration and therefore the calibration frequency seems sufficient. We can then say with caution, that DWD staff did not wait too long to recalibrate their PFR instruments and the instruments have never been in this obsolete calibration status.

It would be interesting to show the influence of the calibration of the CIMEL instruments on the AOD difference ($AOD_{harm\text{-}CIMEL}$ - $AOD_{harm\text{-}PFR}$). But it is not worth to consider then the AERONET Level 2.0 product, since, as explained in subsection 2.2.2 in the analysis of Figure 2.2.3, AERONET Level 2.0 product uses calibration values (V_0) that are interpolated between the last and the next calibration.
An interesting outlook of this study would be to plot the same graphic as Figure 2.2.5 but with AERONET or CÆLIS Level 1.5 products for the $AOD_{harm\text{-}CIMEL}$, since these products use (like PFR does) the (V_0) calibration values of the last calibration.

2.3 PFR/CIMEL intercomparisons on GAW-PFR stations

In this section we investigate how the harmonised AOD computation defined in section 2.1 (AOD_{harm}) can be applied to other stations than Lindenberg (section 2.2) for an AOD comparison that is independent of the retrieval method. For this work, we selected four stations where instruments from AERONET and GAW-PFR are co-located. The stations and data selections are tailored to the purpose of this study, which is focused on the effect of post processing differences for AOD retrieval.



Figure 2.3.1 Map of the stations of the study of intercomparison PFR-CIMEL at some stations that are as well GAW-PFR and AERONET stations

The selected stations are Izaña on the island of Tenerife, Spain, Davos in Switzerland, Hohenpeißenberg in Germany and Valladolid in Spain (see map of Figure 2.3.1 and Table 2.3.1). In this way, we ensure the representation of different conditions. Izaña is the highest and southernmost station, being at an altitude of approximately 2370 m above sea level. Izaña is located on an island in the Atlantic Ocean west of Morocco. As a result, it is most of the time a very clean station with very low AOD, but is often affected by Saharan dust episodes that significantly increase AOD and reduce Ångström Exponent (AE). Davos is an Alpine station at an altitude of approximately 1580 m. It is lower than Izaña and surrounded by densely populated regions, but high enough to maintain pristine conditions typically and north enough not to be affected so frequently and intensely by Saharan dust transport. Hohenpeißenberg is northeast of Davos, a quite similar station, but lower (~990 m) and therefore less pristine. Finally, the station in Valladolid is located at the edge of a middle-sized city (approximately 300 000 inhabitants) at an altitude of approximately 700 m surrounded mostly by plains. It is associated with GAW-PFR through its participation in ACTRIS-CARS (Aerosol, Clouds and Trace Gases Research Infrastructure - Centre for Aerosol Remote Sensing). As GAW-PFR includes mostly background locations, Valladolid is the only urban site where CIMEL and PFR parallel measurements for several years exist. As a result, these stations represent various conditions in terms of aerosol load, size and composition, atmospheric pressure and ozone column, which are components affecting either the post processing of AOD or AOD itself.

Table 2.3.1 Information about stations involved in the study of intercomparison PFR-CIMEL at some stations that are as well GAW-PFR and AERONET stations

Station	Name	Geo-coordinates	Institution	Country	AERONET	GAW-PFR
DAV	Davos	9.85 E, 46.81 N, 1580.0 m	PMOD/WRC	Switzerland	Davos	DAVOS
HPB	Hohenpeißenberg	11.01E, 47.80 N, 995. m	MOHP (DWD)	Germany	HohenpeissenbergDWD	HOHENPEIS-SENBERG
IZO	Izaña	16.5 W, 28.31 N, 2371.0 m	IARC (AEMET)	Tenerife, Spain	Izana	IZAÑA
VLD	Valladolid	4.71 W, 41.66 N, 705.0 m	GOA-UVa (UVa)	Spain	Valladolid	VALLADOLID

2.3.1 Preparation of the dataset and quality analysis

Preparation of the dataset

The datasets include 1 or 2 years per station to ensure sufficient variability of air masses and atmospheric conditions including the entire range of the seasonal cycles. The data selection process differs from the operational procedures used by each network due to the nature of this work. Since the focus is on investigating the effect of post processing by calculating the total atmospheric optical depth and repeating the molecular scattering and gas absorption corrections ensure high confidence of lack of cloudiness in front of the sun or technical issues is necessary, while a reduction on the number of data points has no effect on the study outcome as long as the variety of conditions represented is not too limited. We also used only coincident data between the 2 networks within 30 seconds to maintain consistency among all comparisons.
There are four steps of data selection. The three first ones are using thresholds on the parameters Aerosol Optical Depth (AOD) and Ångström Exponent (AE) that is linked to the aerosol size (a rule of thumb is that if AE is large, the size particles is low, therefore potential water droplets clouds can be filtered out with a threshold on the lowest accepted value of AE).

These are the four steps of data selection:

- Step 1: For AERONET AOD we take only level 2.0 data and applied additional selection criteria that remove extreme or unrealistic values of AOD or AE (retained AODs and pair AEs below 3) and data points where one of the measured wavelengths (up to 1020 nm) is missing, which rejected 2.2% of the initial data. For PFR AOD we initially filtered the AOD according to the automatic algorithm (Kazadzis et al., 2018a).
- Step 2: Reject PFR data through thresholds of AOD and AE to remove extreme or unrealistic values (retained AODs below 3 and AE calculated from fit to all 4 wavelengths below 2.5).
- Step 3: Reject PFR data outside specific thresholds or empirically constructed functions of AOD and AE variability indicators for each station. In particular, those indicators were the 3, 5 and 10-minute running standard deviation and median absolute deviation around each data point. All retained data points being the only measurement within these time windows were rejected. Standard deviation is non-robust, while median absolute deviation robust, providing different information about the variability. The empirical criteria aimed at removing data where this variability was too high and therefore suspicious for cloud contamination. This step retained 88.5% of the PFR data filtered by the automatic algorithm and extreme values (all locations).
- Step 4: The fourth step was to reject PFR data corresponding to measured pressure by the instrument barometer outside a specific range for each station or data where the temperature inside the PFR is outside the tolerance of 0.1 K from the normal temperature of operation of each instrument (which appears for the majority of measurements due to temperature stabilisation). This step retained 97% of the data passing the previous criteria.

After applying the aforementioned criteria to both datasets, we synchronised the datasets and compared coincident data (according to the 30 seconds threshold) for the 2 directly comparable wavelengths (500 and ~865 nm). Then we applied specific thresholds for each station on AOD and AE differences depending on the behaviour of the data (0.025 to 0.04 for AOD depending on

wavelength and station, 0.5 to 1.7 for AE depending on station) to remove any remaining data points with high differences that are very likely to be a result of factors such as thin clouds or imperfect synchronisation under high AOD variability. This final procedure retained 99.3% of the total common data (all locations) that had remained after the separate data screening on each instrument. This shows that the individual criteria per network already rejected the vast majority of data points affected by factors such as clouds. The aim was a dataset as close as possible to one that includes AOD uncertainty induced by post processing, calibration, instrument signal noise, dark signal correction and field of view (details of AOD uncertainty estimations in Deliverable 2.3 - Kazadzis et al., 2024). For this study, we used:

- For Davos (DAV): Two years of data (2019, 2020)
- For Izaña (IZO): Two years of data (2021, 2022)
- For Valladolid (VLD): Two years of data (2022, 2025)
- For Hohenpeißenberg (HPB): only one year of data (2020).

The selection of years was dependent on the data availability passing the above criteria.

Quality estimation of the dataset

The final dataset includes 67486 common data points (all locations) across a large variety of conditions (PFR AOD between 0.01 and 0.77 at 500 nm, AE between 0.04 and 2.15), which we consider sufficient and suitable for the goals of the study.

A first step is to consider the effect of the harmonisation of AOD and verify that there are no stations for which the harmonisation required particularly more corrections than the others. Since we aligned the standards of AOD processing to GAW-PFR, no changes were needed for the PFR dataset: $AOD_{harm} = AOD_{PFR}$. Therefore, we will compare the differences between ($AOD_{AERONET}$) and ($AOD_{harm\text{-}CIMEL}$). The results are shown for channel 500 nm on Figure 2.3.2. The statistics: average bias MBE (Mean Bias Error), average absolute bias MBAE (Mean Bias Absolute Error), and the dispersion around the mean bias RMSE (root means square error of the difference AOD_difference minus MBE) are shown in Table 2.3.2.

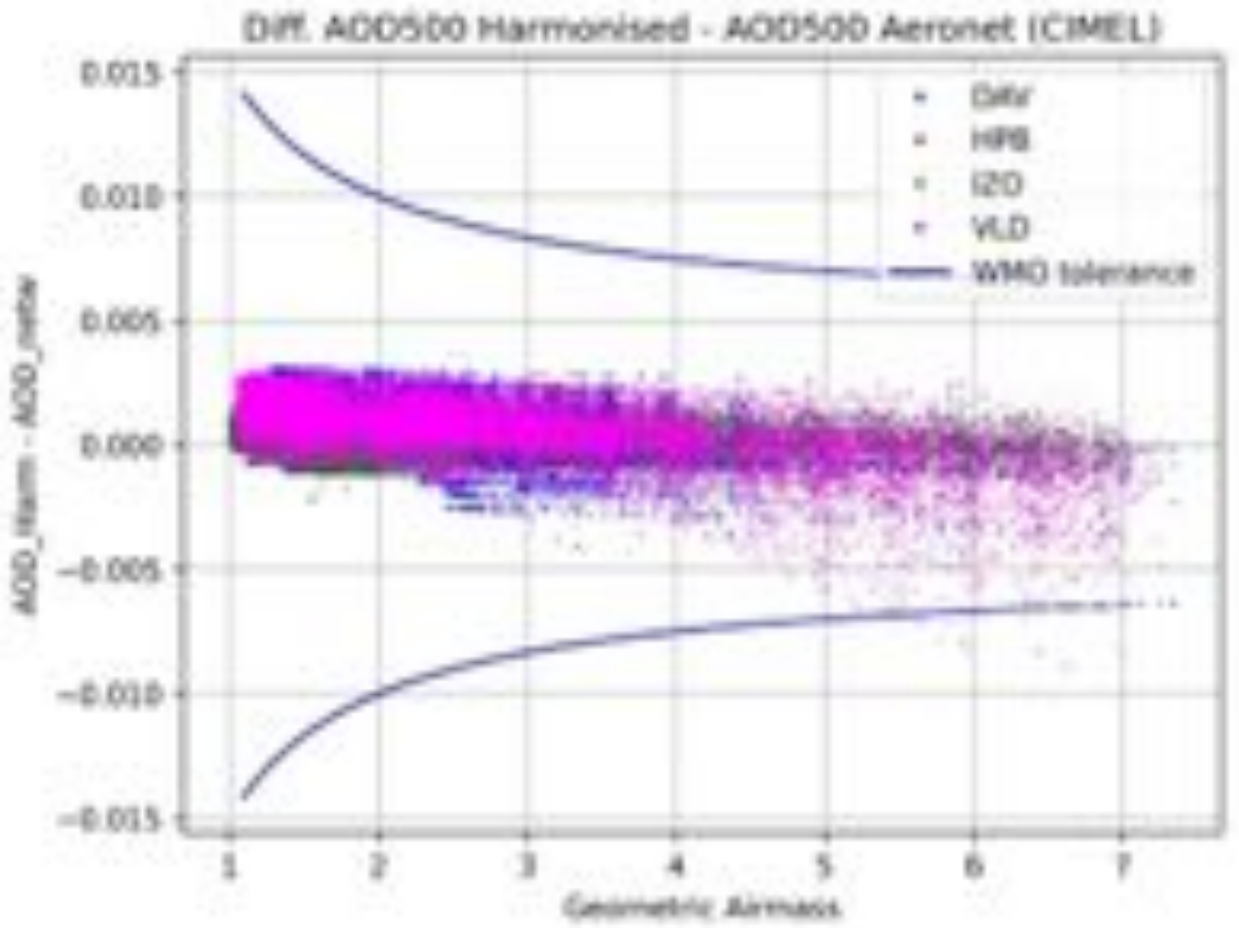


Figure 2.3.2 For all four stations (blue triangles: Davos, red circles: Hohenpeißenberg, green triangles: Izaña, magenta squares: Valladolid), for the 500 nm channel: Differences AOD harmonised minus AOD of network AERONET ($AOD_{harm\text{-}CIMEL}$ - $AOD_{AERONET}$) in dependence of the airmass. Blue lines are the WMO limits of acceptance (WMO tolerance).

Figure 2.3.2 for 500 nm and table 2.3.2 (for both channels) show that the harmonisation correction is similar for all stations and that the corrections are small compared to the WMO criteria of acceptance applied to qualify AOD comparisons: The absolute difference between AOD provided by the network AERONET is almost always below 0.005 and in statistics (see MBAE in table 2.3.2) below 0.0012. Figure 2.3.2 demonstrates that there is no airmass dependence of the harmonisation correction (the scatter distribution of the AOD difference in dependence of airmass is around a horizontal line). The differences are slightly smaller for the channel 870 nm than for the channel 500 nm, this is because the correction of the Rayleigh optical depth ((OD_{Ray}) in E2.4, E2.5 and E2.5a) is large at 500 nm than at 870 nm. Also at 500 nm, the ozone correction is larger than at 870 nm.

Table 2.3.2 Statistics of $AOD_{harm\text{-}CIMEL}$ - $AOD_{AERONET}$ for both wavelengths considered (500 and 870 nm) for all four stations of the study. Parameters shown are: average bias MBE (Mean Bias Error), average absolute bias MBAE (Mean Bias Absolute Error).

WVL(λ)	Station	MBE	MBAE	RMSE(to MBE)
500 nm	DAV	7.122e-04	1.117e-03	1.168e-03
	HPB	8.136e-04	1.045e-03	9.062e-04
	IZO	4.477e-04	6.118e-04	5.793e-04
	VLD	7.461e-04	1.086e-03	1.101e-03
870 nm	DAV	-7.775e-04	7.775e-04	2.647e-04
	HPB	-8.971e-04	8.971e-04	2.557e-04
	IZO	-8.266e-04	8.266e-04	2.270e-04
	VLD	-9.934e-04	9.934e-04	4.965e-04

2.3.2 Harmonised AOD comparison (AOD_{harm}) CIMEL minus PFR in dependence of the airmass. Statistics and analyses

Having verified that the harmonisation is realistic on all four stations and for both spectral channels (500 nm and 870 nm) we can compare the harmonised AOD (AOD_{harm}) issued of CIMEL instrument ($AOD_{harm\text{-}CIMEL}$) to the one issued of PFR instrument ($AOD_{harm\text{-}PFR}$). This comparison is shown on figure 2.3.3 (500 nm channel) and on figure 2.3.4 (870/862 nm channel). The AOD differences are represented in dependence of the airmass. The statistical values are shown in Table 2.3.3 (MBE, MBAE, RMSE).

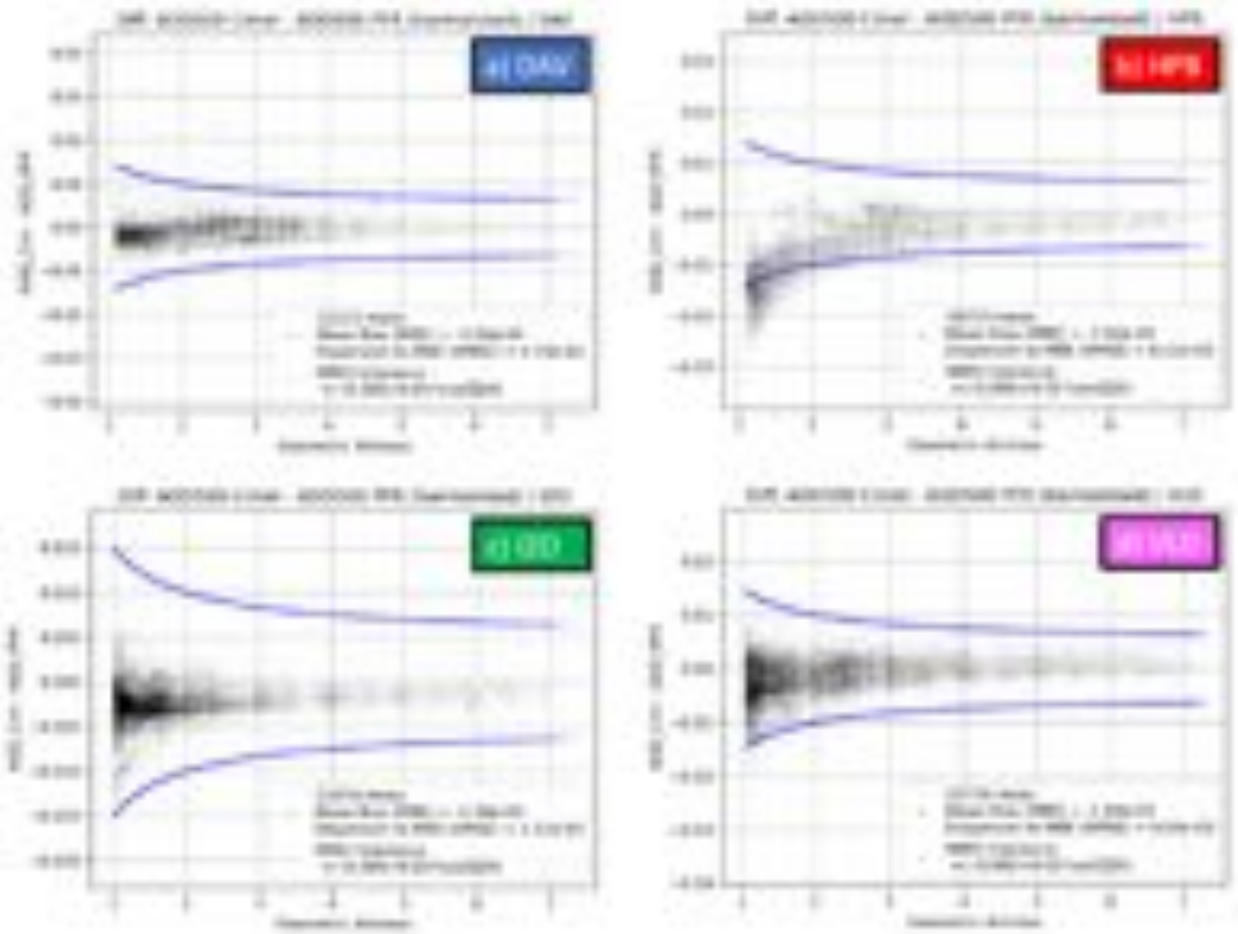


Figure 2.3.3 For each station - a) Davos, b) Hohenpeißenberg, c) Izaña, d) Valladolid, for the 500 nm channel: Differences AOD harmonised for CIMEL instrument minus AOD harmonised for PFR instrument ($AOD_{harm\text{-}CIMEL}$ - $AOD_{harm\text{-}PFR}$) in dependence of the airmass. Blue lines are the WMO limits of acceptance (WMO tolerance).

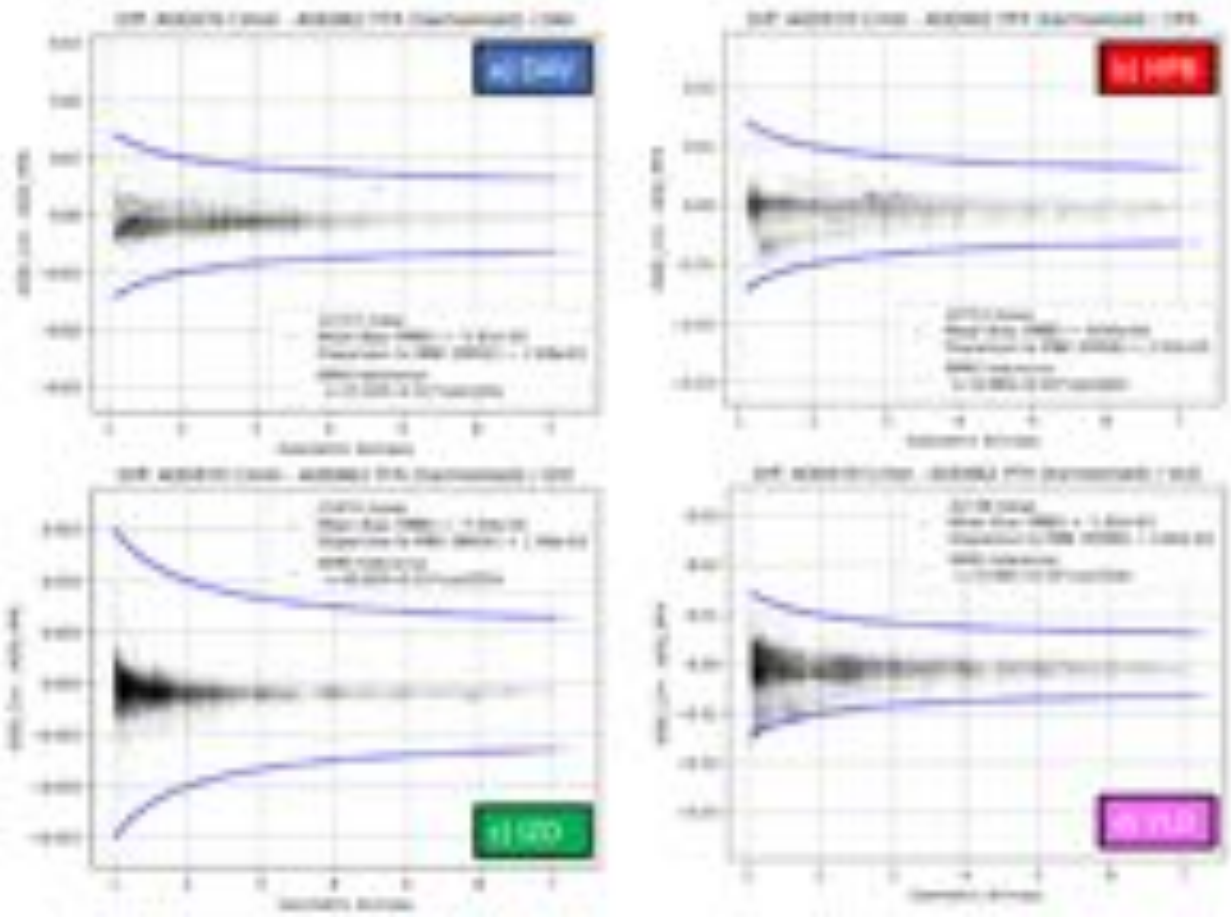


Figure 2.3.4 For each station - a) Davos, b) Hohenpeißenberg, c) Izaña, d) Valladolid, for the 870/862 nm channel: Differences AOD harmonised for CIMEL instrument minus AOD harmonised for PFR instrument ($AOD_{harm\text{-}CIMEL}$ - $AOD_{harm\text{-}PFR}$) in dependence of the airmass. Blue lines are the WMO limits of acceptance (WMO tolerance).

An analysis of these graphics and statistics leads to following statements:

- For both channels, the AOD comparison values are for all stations almost all inside the WMO criteria of acceptance: Only Hohenpeißenberg (HPB) for channel 500 nm has 75,9% only, for Hohenpeißenberg at 862 nm and for the other three stations for both channels, there are always at least 96% of the comparisons that are inside the WMO limits of acceptance.
- At Davos (DAV), for both channels, the mean bias (MBE) is together with Izaña (IZO) the lowest but the dispersion (RMSE to MBE) is together with Valladolid (VLD) the largest of the four stations.
- At Hohenpeißenberg (HPB), for channel 500 nm, there are 24% of the points that are outside of the WMO limits, what is much less than expected (WMO consider that the instruments are matching well if 95 %of the comparisons are inside the WMO limits of acceptance). Most of the points outside of the WMO limits are in the low geometric

airmass domain, revealing a calibration issue from one instrument or the other (CIMEL or PFR) or both of them.

- At Izaña (IZO), for both channels, the dispersion (RMSE to MBE) is very low (the lowest) and the bias (MBE) is together with Davos (DAV) the lowest. A realistic (but nevertheless only hypothetic) explanation is that Izaña is a site at which the Langley Plot calibration is conducted. Therefore, no error due to the standard transfer of calibration throw a transfer photometer can occur.
- At Valladolid (VLD), the dispersion and the bias have some of the highest values of the four stations. This can be explained with the fact that Valladolid is the only urban site of all the four stations and the absolute value of the AOD is the highest of all four stations (with for almost 50 % of the dataset, AOD at 500 nm is > 0.1). Therefore, since we show here an absolute difference of AOD and not a relative one, the AOD difference is consequently higher than for stations with lower absolute values of AOD.
- The AOD difference is decreasing with the airmass. This observation was expected (see subsection 2.1.3 of the method's description). This effect is especially visible for stations in the south of Europe since there, the sun elevation reaches higher values and consequently the airmass reaches lower values, making the photometry less precise (theoretical demonstration in subsection 2.1.3).

Table 2.3.3 Statistics of $AOD_{harm\text{-}CIMEL}$ - $AOD_{harm\text{-}PFR}$ for both wavelengths considered (500 and 870/862 nm) for all four stations of the study. Parameters shown are: average bias MBE (Mean Bias Error), average absolute bias MBAE (Mean Bias Absolute Error), and the percentage of the comparisons for which the AOD difference is lower than the WMO limit of acceptance. In brackets in the WMO limit percentage, is indicated how much more (if positive) or less (if negative) percents of the comparison are in the WMO limits for (AOD_{harm}) comparison in relation to original dataset (AOD_{netw}) comparison,

WVL(λ)	Station	MBE	MBAE	RMSE (to MBE)	%in WMO limit
500 nm	DAV	-9.773e-04	3.387e-03	5.037e-03	96,1 % (+ 0,17 %)
	HPB	-7.809e-03	8.140e-03	6.651e-03	75,9 % (+6,64 %)
	IZO	-2.812e-03	3.063e-03	2.249e-03	99,9 % (+ 0,11 %)
	VLD	-2.438e-03	3.595e-03	4.197e-03	98 % (+ 0,93 %)
	DAV	1.862e-04	1.977e-03	3.538e-03	97,6 % (+ 0,31 %)

870/862 nm	**HPB**	-9.364e-05	2.013e-03	2.926e-03	99,5 % (- 0,02 %)
	IZO	7.287e-05	9.615e-04	1.486e-03	99,9 % (+ 0.01 %)
	VLD	-6.086e-04	2.666e-03	3.914e-03	98,1 % (- 0,58 %)

Table 2.3.3 also shows in the last columns in brackets what is the gain in quantity of comparison points in % that match the WMO criteria of acceptance from the AOD comparison with the original dataset (AOD_{netw}) to the harmonized dataset (AOD_{harm}). For Hohenpeißenberg (HPB) at 500 nm, we have a significant improvement. For other sites and wavelengths, the improvement is much smaller. It was expected that the (AOD_{harm}) dataset matches better between the instruments than the (AOD_{netw}) dataset does. But in theory it is possible that for some or many comparison points, (AOD_{netw}) better matches than (AOD_{harm}) does for instance if some calibration/radiation measurement errors are compensated by AOD computation differences in the opposite direction.

2.3.3 Evolution of the difference of harmonised AOD (AOD_{harm}) CIMEL minus PFR on a long time series.

We now want to show the time evolution of the AOD difference (of course on AOD harmonised: (AOD_{harm})) between CIMEL ($AOD_{harm\text{-}CIMEL}$) and PFR ($AOD_{harm\text{-}PFR}$).
In the methodology section (2.1) we demonstrated in subsection 2.1.3 that it is necessary to consider the AOD difference at the same value of airmass, that means the same value of solar zenithal angle (SZA) or solar elevation. We decided to fix this value of SZA to 70° in order to have some measurements for almost all days of the dataset also in winter in the stations situated at the highest latitudes (DAV: Davos and HPB: Hohenpeißenberg).

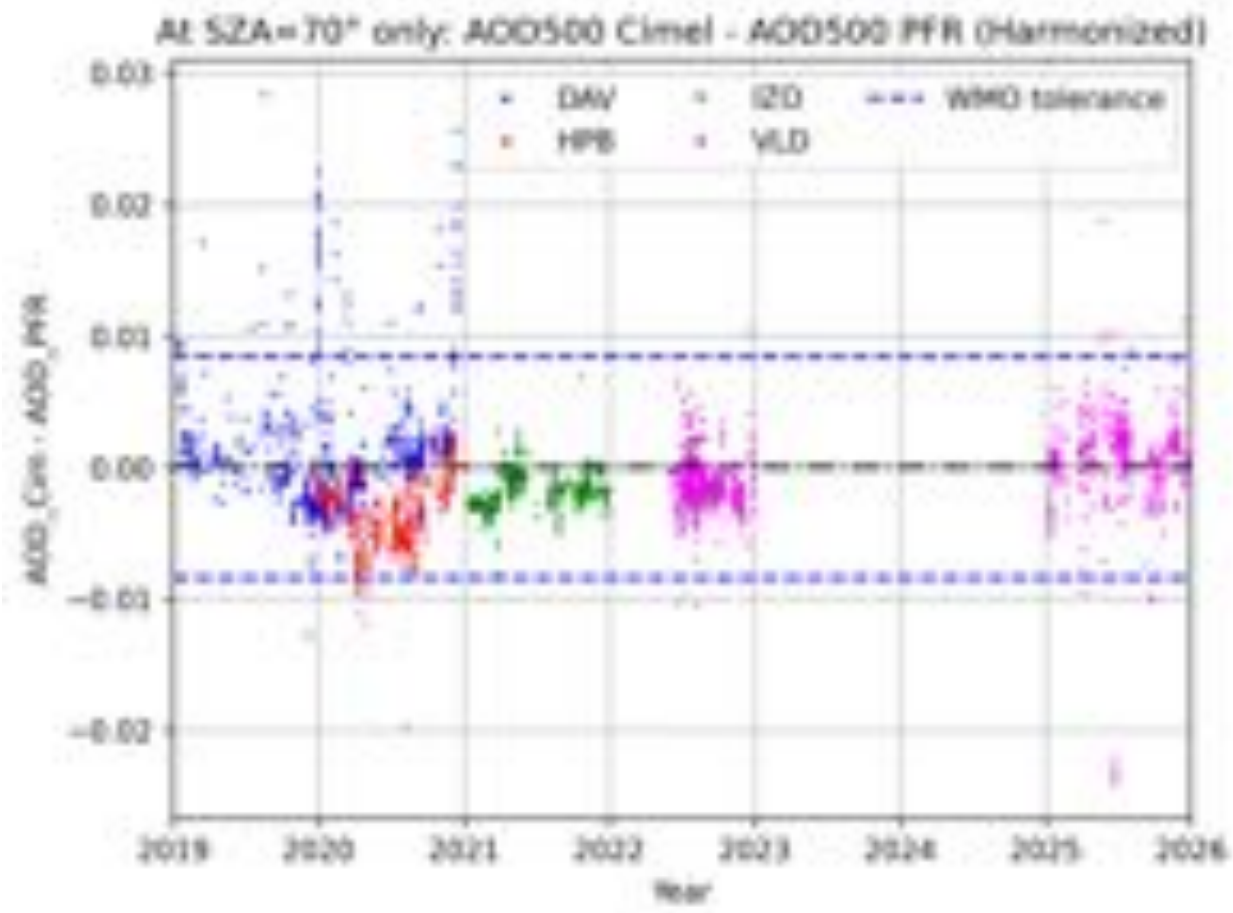


Figure 2.3.5 For channel 500 nm, for SZA = 70° only, for all stations (blue triangles: Davos, red circles: Hohenpeißenberg, green triangles: Izaña, magenta squares: Valladolid): Time series of the differences of AOD harmonised for CIMEL instrument minus AOD harmonised for PFR instrument ($AOD_{harm\text{-}CIMEL}$ - $AOD_{harm\text{-}PFR}$) in dependence of time. Blue dashed lines are the WMO limits of acceptance for SZA = 70°.

Figure 2.3.5 shows the complete time series (2019 - 2025) of the evolution of the harmonised AOD difference ($AOD_{harm\text{-}CIMEL}$ - $AOD_{harm\text{-}PFR}$) at 500 nm for the datasets of all stations. The observations of subsection 2.3.2 are still visible: Low absolute differences at Izaña (IZO), large absolute difference (dispersion) at Valladolid (VLD) and Hohenpeißenberg (HPB, red) that can be at the WMO limit or outside of it.
For Hohenpeißenberg, we notice that beginning 2020, the bias $AOD_{harm\text{-}CIMEL}$ - $AOD_{harm\text{-}PFR}$ is pretty low (a third of the WMO limits) and again at the end of 2020. But in the middle of the year, this bias is larger. This can be a calibration issue. An outlook of this study would be to look at the serial numbers of the instrument involved (as well CIMEL and PFR) and to check when the calibration of these instruments has been done. Probably is one (or both) of the instruments

involved having at the middle of 2020 an obsolete calibration and this problem has been solved in autumn 2020.

2.4 Summary of the AOD comparison on the harmonised AOD dataset

In this deliverable (and especially in this part -part 2, sections 2.2 and 2.3) we assess the differences of AOD from different photometers and photometer types (PFR, Prede, and CIMEL) retrieved by the same or different retrieval algorithms. To account for instrumental factors—such as radiation measurements, calibration issues, and calibration stability—we first needed to remove differences in the AOD datasets caused by the different methods used to calculate AOD from total optical depth (TOD; see Equation (E2.7)).These methodological differences arise because data from different instrument types are processed by different networks: AERONET and additionally, at some stations, CÆLIS for CIMEL; SKYNET for Prede; and GAW-PFR for PFR. To avoid these differences, we defined a common standard AOD, (AOD_{harm}) calculated from TOD using a methodology and input-component amounts that are independent of the network from which the data originate. (AOD_{harm}) is defined in Equation (E2.8).
Using (AOD_{harm}), we analysed the Lindenberg AOD dataset (section 2.2) and found good agreement between the PFR and CIMEL instruments. We also identified periods—for example, in 2022—when either the CIMEL or PFR instrument may have experienced hardware issues (e.g., calibration, sun pointing, filters damaging). The CÆLIS dataset provided a valuable complement to the established networks (AERONET, GAW-PFR, and SKYNET), as it enabled us to compare the AOD values from the two CIMEL instruments directly. This helped us investigate the differences between CIMEL and PFR. In addition, the ($AOD_{harm\text{-}CIMEL}$- $AOD_{harm\text{-}PFR}$) comparison showed when and how the Prede instruments at Lindenberg diverged substantially from the other two instrument types, suggesting several opportunities for further investigation.
In section 2.3, we extended the CIMEL–PFR analysis to stations equipped with both instrument types: Davos, Hohenpeißenberg, Izaña, and Valladolid. ($AOD_{harm\text{-}CIMEL}$- $AOD_{harm\text{-}PFR}$) comparisons, which are free from artifacts caused by differences in the AOD calculation methods used by AERONET and GAW-PFR (including differences in equations, coefficients, and gas amounts), allowed us to discuss possible instrumental issues and site-related differences in measurement and calibration conditions. Future work on the section 2.3 analysis could include examining multiple CIMEL instruments operating in parallel at the same sites (Valladolid and Izaña) by incorporating the CÆLIS dataset. Another avenue would be to investigate additional stations equipped with both PFR and CIMEL instruments, such as Sodankylä in northern Finland, operated by the Finnish Meteorological Institute (FMI), and Ny-Ålesund in Svalbard.

3. Harmonisation and comparison experiments during FRC-VI campaign

3.1 FRC-V and FRC-VI campaigns

Field campaigns bringing together a large number of different instruments to perform measurements simultaneously and under the same conditions are key to understanding the discrepancies between instruments and processing algorithms. In addition, they allow the validation of procedures and techniques. This knowledge is essential to establish the state of the art of solar radiation measurements: it sheds light on the uncertainties of the obtained quantities and the limitation of the measurements and retrievals, and suggests improvements as well as important issues that should be addressed.

3.1.1. FRC (Filter Radiometer Comparisons) campaigns in Davos

Deliverable D1.1 (Doppler et al. 2023) from HARMONIA's WG1 compiles information on 23 campaigns from the period 2014-2022, that is, prior to the establishment of HARMONIA, and highlights six of them. Of these campaigns, the most significant regarding photometers is the FRC (Filter Radiometer Comparison). Nominally every 5 years, the WMO (World Meteorological Organisation) organises three campaigns which are simultaneously carried out at the PMOD/WRC in Davos (Switzerland). Each campaign focuses on a different type of instrument: the FRC (Filter Radiometer Comparison), the IPC (International Pyrheliometer Comparison) and the IPgC (International Pyrgeometer Comparison). During these campaigns, national meteorological centres and manufacturers of radiometric equipment install their instruments to calibrate them against the reference. Afterwards, these centres organise regional calibration campaigns to ensure traceability within their region. The descriptions about FRC-IV (2015) and FRC-V (2021) are presented in HARMONIA deliverable D1.1 (Doppler et al. 2023).

The FRC-V took place from 27 September to 25 October 2021 (Kazadzis et al. 2023, Doppler et. al. 2023). Several sun-photometers from the main aerosol networks participated, including 13 PFRs (10 + the WORCC reference triad) belonging to the WMO/GAW network, 4 CIMEL CE-318 from AERONET, 2 Prede POM sky radiometers from SKYNET and a CW-193 from CARSNET (China Aerosol Remote Sensing Network). Therefore, these campaigns offer an exceptional opportunity to compare sun-photometer measurements belonging to different networks.

To date, the most recent edition of these campaigns is the FRC-VI, which took place in 2025; as such, it has not yet been mentioned in any HARMONIA deliverable. Therefore, we provide a brief overview of it here.

3.1.2. Introduction to the FRC-VI (Sixth WMO Filter Radiometer Comparison)

The sixth Filter Radiometer Comparison (FRC-VI) campaign was organized by the PMOD/WRC and supported by the World Meteorological Organization (WMO). Analogously to the previous FRC editions, it was conducted in parallel with the International Pyrheliometer Comparison (IPC, which hosted 157 visiting instruments) and the International Pyrgeometer Comparison (IPgC) involving 35 instruments. FRC-VI was held in Davos, Switzerland from 19 September to 19 October 2025. During this period, there were 13 days with at least 4 hours of sunshine, with AOD at 500 nm varying from 0.015 up to 0.069, which is representative for the Davos location. 14 institutes participated, representing ten international and national AOD networks (AERONET, GAWPFR, ACTRIS-EU, SKYRAD-EU, SKYRAD-JP, SURFRAD, CARS-China, Finland, Germany and Sweden) with 39 filter radiometers and spectroradiometers (16 different instrument types) present, including mostly sun-pointing, but also shadowband radiometers (Figure 3.1.1).



Figure 3.1.1 Pictures of the instruments that participated in FRC-VI (Sep-Oct, 2025)

Measurements from participating radiometers were evaluated having as a reference the WMO/WORCC (World Optical Depth Research and Calibration Center) GAWPFR-TRIAD. The filter radiometers and spectroradiometers provided their AOD data using their own post processing algorithms. Additional data (e.g., pressure, ozone) have been provided by PMODWRC. The campaign followed the recommendations of WMO/GAW experts report (WMO/TD-No. 1287. 2005), which calls for:

- More than 1000 data points with AOD at 500 nm between 0.04 and 0.20;
- A minimum duration of 5 days;
- Traceability requires 95% compliance within WMO limits on AOD differences (± (0.005 + 0.01/m)).

Comparisons have been performed in the four PFR measuring wavelengths (368nm, 412nm, 500nm, 862nm). Whenever possible, the Ångström Exponents (AE) calculated from second order polynomial fits of the PFRs covering a range from 340nm to 1640nm are also compared.

In the spectral range 368 nm to 412 nm, at least 78% of instruments met the WMO traceability criteria when compared with the GAWPFR-TRIAD. This percentage increased from 440 nm to 1020 nm, ranging from 83% to 100%. An exception is AOD at 500 nm, with compliance as low as 74%; this increases to 80% when the handheld filter radiometers are excluded, dropping to 50% for the 340 nm wavelength. Comparison at 500 nm is presented in Figure 3.1.2. Detailed results of the FRC-VI will be presented in a WMO report to be published by the end of 2026.

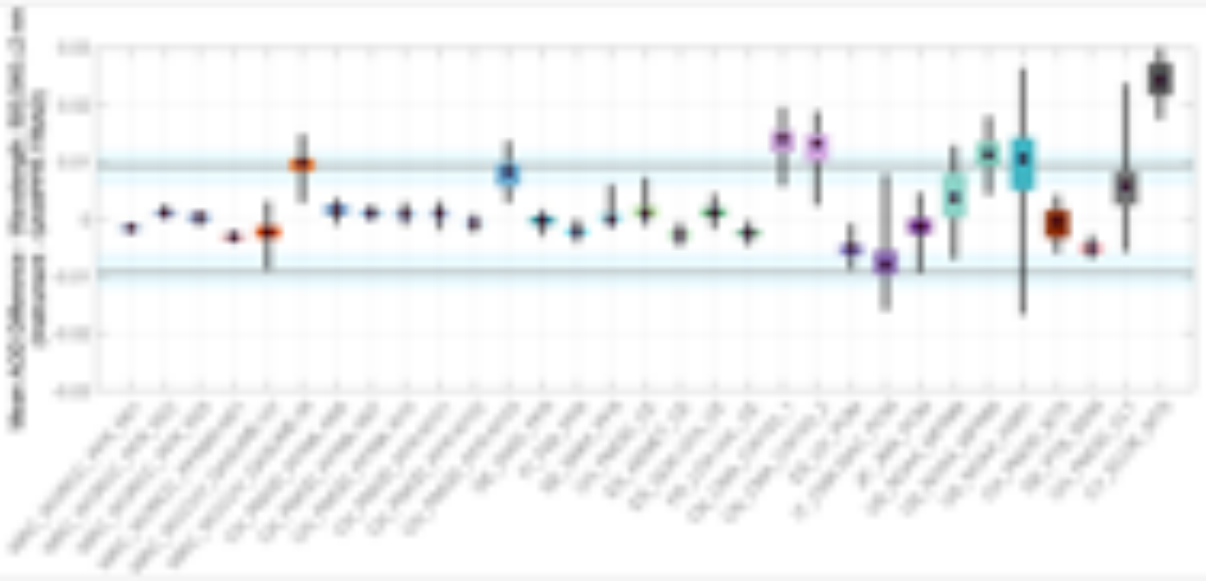


Figure 3.1.2 AOD difference of each instrument listed in the horizontal axis with the GAWPFR-TRIAD. The open circles represent the median of the difference of each instrument to the reference at each wavelength over the 13 FRC-VI days. The coloured boxes span the 25th to 75th percentiles, while the black vertical lines represent the minimum and maximum values of the distribution, excluding the outliers (99.3% coverage). The black horizontal lines represent the average WMO limits, with light blue representing the range of these limits, based on the airmass change during the campaign.

3.2 Outcomes from the FRC-VI campaign: harmonisation of AOD measurements from Prede and CIMEL instruments

In this section, the results of the validation of the Sunrad algorithm against AERONET's product using Prede and CIMEL data from the FRC-VI campaign are described. This work was part of the STSM "Comparison of AOD and aerosol retrievals collected during the FRC-VI campaign in Davos and validation of improved data processing and calibration algorithms" carried out by Meritxell Garcia Suñer under the supervision of Dr. Stelios Kazadzis.

3.2.1. The Sunrad algorithm

The Sunrad algorithm, as described in Estellés et al. 2012 is one of the two modules that constitute the open-source package ESR.pack. It is used to retrieve AOD, AE and the total column of water vapor (TCWV) from direct sun extinction measurements. The other module included in ESR.pack inverts the sky radiance to obtain properties such as the volume size distribution, refractive index or asymmetry parameter.

The Sunrad algorithm was developed in order to enable synergistic analyses between instruments from different networks. It consists of two main routines, *dsform* and *dsproc*. The aim of *dsform* is to convert raw data files from CIMEL or Prede instruments to the Sunrad-specific format. For this task, two configuration files are used: *dsform.par*, which contains information about the calibration coefficients, available wavelengths and the characteristics of the measurement site; and *meteo.dat*, where the NO_2 , O_3 , TCWV, temperature and pressure values can be specified. Once the raw data have been formatted, they are processed using the *dsproc* routine, which yields the AOD, AE (Ångström Exponent) and TCWV values. The International SKYNET Data Center (ISDC) has established a standard configuration for data processing using the Sunrad algorithm. From now on, this version of the algorithm will be referred to as "Sunrad ISDC".

3.2.2. Instrumentation

In this analysis, data from the CIMEL CE-318 #1144, belonging to the University of Lille, have been processed using the Sunrad algorithm. The AERONET retrievals for this CIMEL have been taken as the reference for the comparison. Furthermore, measurements collected by the Prede POM-01 from Burjassot (Valencia, Spain), University of Valencia, hereafter referred to as the "UVEG Prede", and the lunar Prede POM-01 from Tor Vergata (CNR/ISAC, Rome), hereafter referred as "CNR Prede" have also been processed and compared to AERONET's retrievals for CIMEL #1144. The data collected by the third Prede, a POM-02 belonging to the Japan Meteorological Agency (JMA), will be analysed in a future outlook study.

It is important to mention the incident that occurred between the UVEG and CNR Prede instruments: During a control test, the UVEG Prede's collimator collided with that of the CNR Prede, causing the base of the former to shift. This led to pointing problems in the UVEG Prede. For this reason, data from this instrument from 9 October onwards are not taken into account in this analysis. Following this incident, the UVEG Prede has continued to experience some problems and is not operational at the time of writing, as issues with the transmission belt have been detected.

3.2.3. Measurement days

Weather conditions during the FRC-VI campaign were, on the whole, unfavourable, with many days affected by rain, snow or cloud cover (Figures 3.2.1a and b). Fortunately, 28 and 29 September were clear, with a pristine atmosphere as the rain from the previous days had washed away the aerosols. Furthermore, 2 and 3 October were also particularly clear. Therefore, data from these four days were used for the calibration transfer from CIMEL #1144 to the UVEG Prede, as very stable measurements are required for the processing to be carried out successfully. Given

the lack of full days with optimal measurement conditions, and taking into account the improved weather forecast for the days following the campaign, it was decided to extend it until 19 October.



Figure 3.2.1 a) The PMOD/WRC esplanade on a snowy day, where all the instruments involved in the FRC-VI campaign were set up. b) A closer view of the three Prede instruments (on the table, from left to right: the JMA, UVEG and CNR Prede instruments), the PFR instruments (to the left of the table) and the CW-193 (far right).

3.2.4. Assessing the differences between AERONET and SKYNET networks using the Sunrad algorithm.

The main goal of this subsection is to identify and evaluate to what extent the differences in instrumentation and methodology between the AERONET and SKYNET networks affect the retrieval of AOD. In particular, we have studied the influence of the retrieval algorithm, the instrumentation and the calibration methodology. This analysis was possible thanks to the Sunrad algorithm, which allows full control of the configuration for processing CIMEL or Prede raw data. The AOD retrieved using Sunrad has been compared to AERONET's Level 1.5 data from CIMEL #1144 (Level 2.0 was not available at the time the analysis was carried out).

In the first study, the CIMEL #1144 raw data were processed through Sunrad, using the calibration coefficients of this instrument, so the discrepancies with AERONET's dataset can be entirely attributed to the different algorithms used.

Once the effect of the algorithm on the retrieval had been examined, we processed Prede raw data using the calibration coefficients transferred from CIMEL #1144. In this way, the two factors that determined the differences between the Sunrad and AERONET retrieved AOD were the instrumentation (as data collected by a Prede are compared to measurements from a CIMEL) and the algorithm used, which had been analysed in the previous case.

Finally, Prede raw measurements have been processed using Prede's calibration and compared to AERONET's CIMEL #1144 retrievals. Therefore, apart from the instrumentation and the

algorithm applied, the other element that caused a difference in the AOD retrieval was the calibration method followed.

3.2.4.1. Sunrad retrieval on CIMEL

Measurements from the CIMEL instrument #1144 collected from 17 September to 18 October have been processed with Sunrad ISDC using the default *meteo.dat* file. The channels available for the processing are 340, 380, 440, 500, 675, 870 and 1020 nm (the 1640 nm channel is not yet well characterised in the Sunrad algorithm, so we decided not to include it in the analysis). It is important to consider the effect of temperature on the calibration coefficients, as larger differences in the retrievals appear, especially at 1020 nm, when this effect is not taken into account.
The discrepancies between the obtained AOD for the available channels and the AOD from AERONET's Level 1.5 retrievals are shown in Figure 3.2.2. In particular, Figures 3.2.2a and 3.2.2b show the scatter plots for the 340 and 1020 nm channels, respectively, with the ideal agreement marked by the pink dashed line with slope 1. In addition, the time evolution of the AOD differences has also been studied (see Figures 3.2.2c and 3.2.2d for the 340 and 1020 nm channels, respectively). Finally, the AOD differences have been analysed quantitatively by calculating the main statistical parameters: the Root Mean Square Error (RMSE), the standard deviation of the differences, the Mean Bias Deviation (MBD), the 90th percentile (P90) and the correlation coefficient R^2. All these results are summarised in Table 3.2.1.
According to Sinyuk et al. 2012 and Sinyuk et al. 2020, the estimated errors in the retrieval of AOD are 0.01 in the visible range and 0.02 in the UV. Therefore, based on the AOD difference statistics in Table 3.2.1, there is very good agreement between the AERONET and Sunrad procedures for the calculation of AOD. The largest discrepancies are obtained at the 340 nm channel (see also Figures 3.2.2a and 3.2.2c). This is an expected result, as the determination of the calibration coefficients and the characterisation of the filters and the gas absorption are more difficult in the UV. However, since these discrepancies are not significant, it can be concluded that there are no important differences between the AOD determined with Sunrad and with AERONET's algorithm from the same dataset.

Table 3.2.1 Statistical parameters of the AOD differences between Sunrad and AERONET ($\Delta AOD = AOD_{Sunrad} - AOD_{AERONET}$) at the available channels: Root Mean Square Error (RMSE), Standard Deviation of the differences (DIFF STD), Mean Bias Deviation (MBD), 90th percentile (P90) and correlation coefficient R^2.

	RMSE	DIFF STD	MBD	P90	R^2
ΔAOD_{340}	0.0070	0.00295	0.00635	0.0110	0.9654
ΔAOD_{380}	0.0025	0.00153	0.00159	0.0045	0.9815

ΔAOD_{440}	0.0014	0.00083	0.00083	0.0025	0.9909
ΔAOD_{500}	0.0007	0.00045	-0.00001	0.0009	0.9942
ΔAOD_{675}	0.0005	0.00019	-0.00047	-0.0002	0.9990
ΔAOD_{870}	0.0004	0.00008	-0.00039	-0.0003	0.9997
ΔAOD_{1020}	0.0012	0.00049	0.00056	0.0017	0.9189

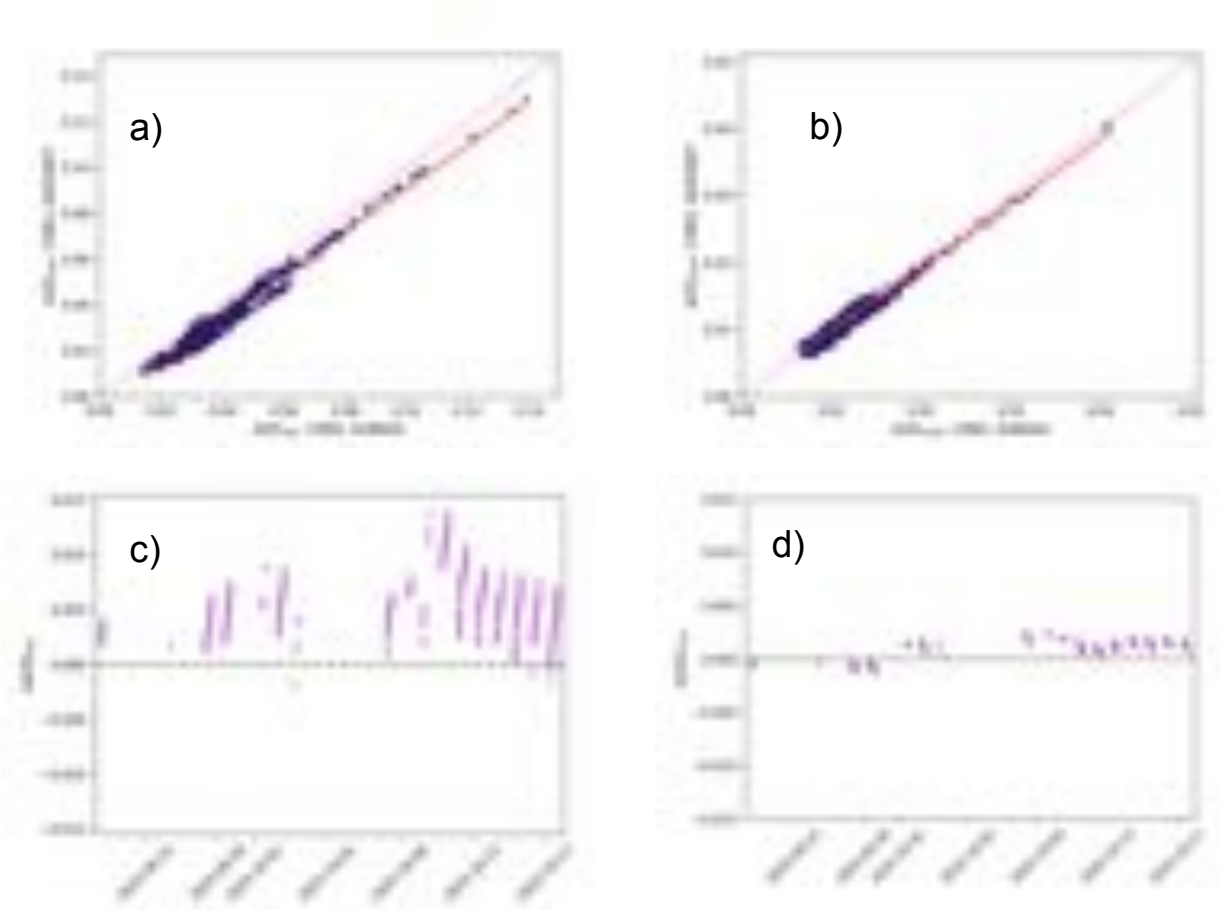


Figure 3.2.2 Scatter plots of AOD at 340 nm (a) and 1020 nm (b) obtained by AERONET (y-axis) and by Sunrad applied to CIMEL data (x-axis). The pink dashed line has slope 1 and represents perfect agreement, while the red line shows the linear regression of the data points. In a), the regression line is $AOD_{AERONET}$ = 0.950*AOD_{SUNRAD} -0.004, while in b) it is $AOD_{AERONET}$ = 0.961*AOD_{SUNRAD} -0.0001. Figures c) and d) show the time evolution of the AOD differences at 340 and 1020 nm, respectively, with the green dashed line representing perfect agreement.

3.2.4.2. Sunrad retrieval on Prede using calibration transferred from CIMEL

Once we had evaluated the differences between the Sunrad and AERONET algorithms in obtaining AOD, we analysed the role of the instrumentation itself in the determination of this quantity. To this end, the UVEG Prede raw data from 22 September to 8 October have been processed using Sunrad ISDC, with the default *meteo.dat* file and applying the calibration coefficients transferred from CIMEL #1144. The transfer was carried out following the relation:

$$V'_{\lambda} = V_{\lambda} \frac{R_{\lambda,PREDE}}{R'_{\lambda,CIMEL}} \quad \text{(E3.1)}$$

where V'_{λ} are the transferred coefficients for the Prede at wavelength λ, and V_{λ} the calibration coefficients of CIMEL #1144 at the corresponding wavelength. It is important to mention that only the wavelengths common to the CIMEL and the Prede can be considered for the transfer, namely 500, 675, 870 and 1020 nm. $R_{\lambda,PREDE}$ represents the raw Prede measurements, whereas $R'_{\lambda,CIMEL}$ indicates the raw CIMEL #1144 measurements corrected for temperature. At temperature T (recorded by CIMEL #1144), with $R_{\lambda,CIMEL}$ the raw CIMEL #1144 measurements at wavelength λ and $k_{T,\lambda}$ the corresponding temperature coefficients (obtained from the CÆLIS webpage: https://goa.uva.es/caelis/), the corrected irradiance measurements are obtained from

$$R'_{\lambda,CIMEL} = \frac{R_{\lambda,CIMEL}}{1 + k_{T,\lambda}(T - 25)} \quad \text{(E3.2)}$$

The calibration transfer (equation (E3.1)) has to be applied to datasets with small variations between the measurements (i.e., corresponding to stable sunny days with no clouds) in order to minimise the errors introduced in the procedure. Therefore, we considered only data from 28 and 29 September and 2 and 3 October. In addition, we used raw CIMEL and Prede measurements differing by a maximum of 5 seconds. A total of 25 pairs of Prede-CIMEL irradiance measurements met these requirements, which allowed us to compute 25 values of V'_{λ}. Finally, the mean of these V'_{λ} was calculated and applied in the Sunrad procedure. Figure 3.2.3 shows the computed V'_{500} for the days considered, and Table 3.2.2 displays the mean V' for each wavelength, as well as the standard deviation and the relative dispersion. Higher variability was found at 500, 870 and 1020 nm. In fact, we concluded that the available dataset poses some challenges when it comes to finding matching measurements for the calibration transfer, due to the presence of clouds and the time lag between Prede and CIMEL measurements. Furthermore, the filter differences between the CIMEL and Prede can be another important error source.

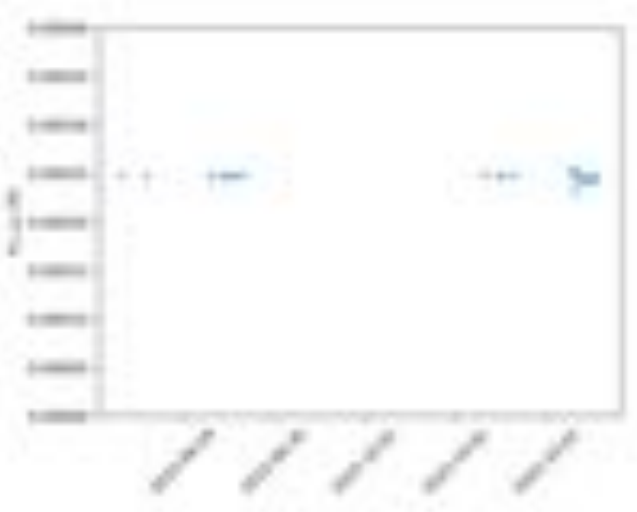


Figure 3.2.3 Time evolution of the V'_{500} calibration coefficients for the UVEG Prede, transferred from CIMEL #1144.

Table 3.2.2 Mean coefficients transferred from CIMEL #1144 to the UVEG Prede, together with the standard deviation and the relative dispersion (ratio between the standard deviation and the mean transferred coefficient) for each wavelength.

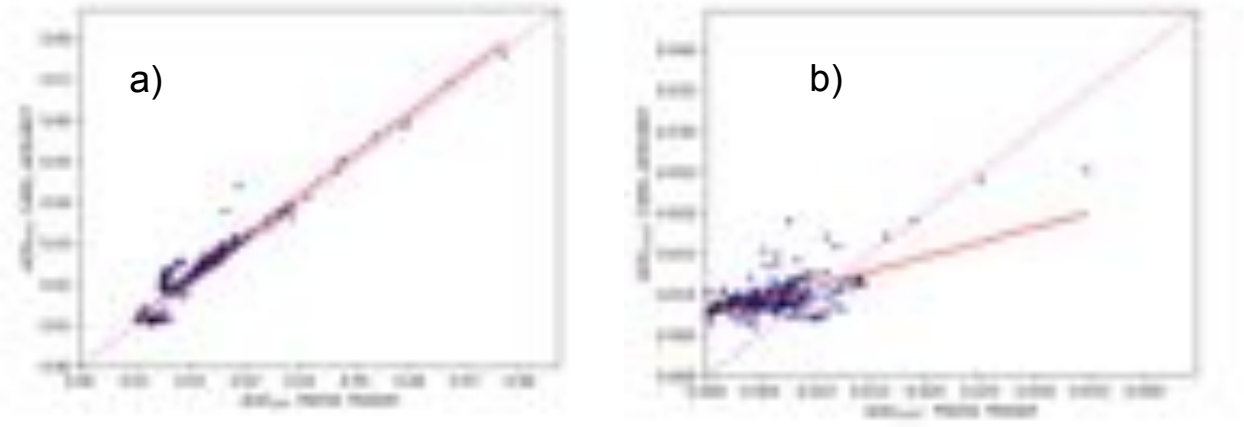
	$V'(\times 10^{-4}\ A)$	$\sigma(V')$ ($\times 10^{-6}\ A$)	$\sigma(V')/V'(\%)$
500 nm	2.47	4.12	1.67
675 nm	3.76	4.54	1.21
870 nm	2.31	3.65	1.58
1020 nm	1.02	1.63	1.60

The transferred calibration coefficients in Table 3.2.2 have been implemented in Sunrad to process the raw UVEG Prede data. Analogously to subsection 3.2.4.1, Figures 3.2.4a and 3.2.4b show the scatter plots to assess the linearity between the AOD obtained by Sunrad and AERONET; Figures 3.2.4c and 3.2.4d depict the evolution of the AOD differences over time; and Table 3.2.3 provides a quantitative analysis of these differences by displaying the main statistical parameters. Overall, the discrepancies between the calculated AOD are within the errors estimated for the retrieval of this quantity. However, they are higher than expected, especially at 1020 nm. The small R^2 at 870 and 1020 nm may be related to the low variability in AOD due to clear-sky conditions. As discussed above, the instrumentation induces certain differences in the retrievals, but the difficulties found in the calibration transfer may be the main reason for the AOD

discrepancies. This hypothesis is supported by the fact that Sunrad underestimates AOD with respect to AERONET at every wavelength (negative MBD in Table 3.2.3), which may be related to the applied calibration coefficients.

Table 3.2.3 Statistical parameters of the AOD differences between Sunrad and AERONET ($\Delta AOD = AOD_{Sunrad} - AOD_{AERONET}$) at the available channels after the CIMEL-Prede calibration transfer: Root Mean Square Error (RMSE), Standard Deviation of the differences (DIFF STD), Mean Bias Deviation (MBD), 90th percentile (P90) and correlation coefficient R^2.

	RMSE	DIFF STD	MBD	P90	R^2
ΔAOD_{500}	0.0029	0.0019	-0.0015	0.0021	0.9163
ΔAOD_{675}	0.0030	0.0015	-0.0026	-0.0006	0.9078
ΔAOD_{870}	0.0029	0.0015	-0.0018	0.0018	0.4873
ΔAOD_{1020}	0.0045	0.0023	-0.0033	0.0014	0.3907



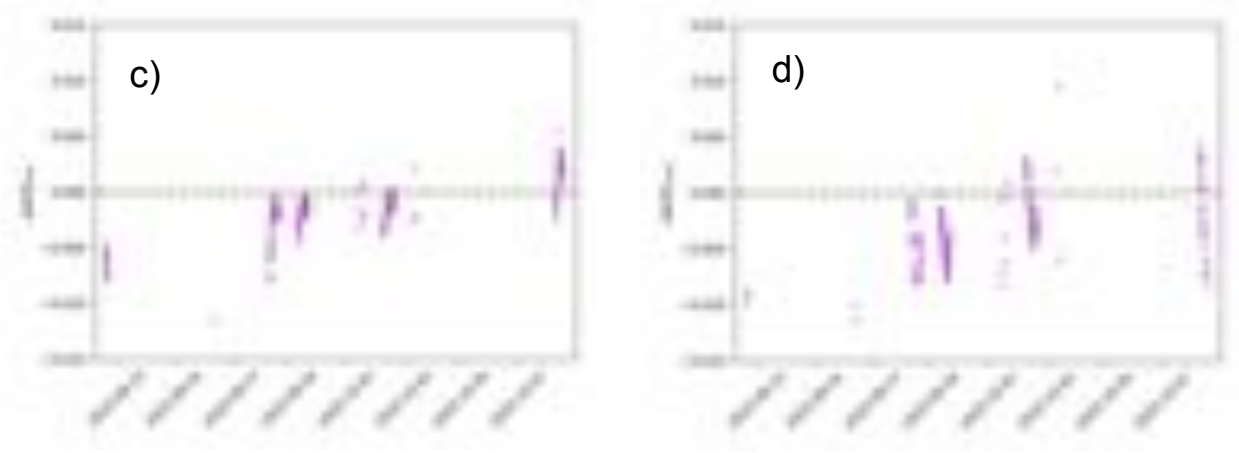


Figure 3.2.4 Scatter plots of AOD at 500 nm (a) and 1020 nm (b) obtained by AERONET (y-axis) and by Sunrad applied to UVEG Prede data with the CIMEL-transferred calibration (x-axis). The pink dashed line has slope 1 and represents perfect agreement, while the red line shows the linear regression of the data points. In a), the regression line is $AOD_{AERONET} = 1.009\ AOD_{SUNRAD} + 0.001$, while in b) it is $AOD_{AERONET} = 0.361\ AOD_{SUNRAD} - 0.007$. Figures c) and d) show the time evolution of the AOD differences at 500 and 1020 nm, respectively, with the green dashed line representing perfect agreement.

3.2.4.3. Sunrad retrieval on Prede data and Prede calibration

- UVEG Prede (from UVEG, Burjassot - Valencia):

Finally, UVEG Prede measurements collected from 22 September to 8 October have been processed using Sunrad ISDC, with the default *meteo.dat* file and applying the calibration coefficients obtained with the Updated Improved Langley Plot (UILP) method (Kumar et al. 2026). Given the problems that the UVEG Prede experienced from 9 October onwards, only the pre-campaign calibration coefficients (i.e., from September) were available for the computation.
When comparing the AOD obtained from Sunrad in this configuration with AERONET's CIMEL #1144 retrievals, the discrepancies are related not only to the algorithm and the instrumentation, but also to the calibration applied. In the previous subsection, despite some difficulties in the calibration transfer related to the small number of simultaneous measurements, the Prede data were processed using a calibration derived from CIMEL #1144. In this subsection, however, the calibration applied to the two datasets are completely independent, which introduces a new source of discrepancies when comparing the retrieved AOD.
Figures 3.2.5a and 3.2.5b show the scatter plots of the Sunrad and AERONET retrieved AOD at 500 and 1020 nm, respectively. In addition, Figures 3.2.5c and 3.2.5d depict the AOD differences

as a function of the air mass, m. The WMO limits are also included. These serve as an indicator of the traceability of the measurements, and are given by

$$WMO_{\pm}(m) = \pm(0.005 + \frac{0.01}{m}) \quad \text{(E3.3)}$$

The statistics computed to quantify these differences can be found in Table 3.2.4. It is important to note that the 340 nm channel was not used in the calculation of AOD with Sunrad in the case of the UVEG Prede, as we found that the filter for this channel was degraded, which affected the calibration of the other channels. We attempted to resolve this issue by computing a new set of Solid View Angles (SVA). However, the new SVA values did not significantly improve the results, so we concluded that the best option was to remove this channel from the calculation.

The discrepancies between the AOD calculated with Sunrad and that provided by AERONET are similar to those obtained in the previous analysis. As discussed, we expected smaller differences when processing Prede measurements through Sunrad with the CIMEL-transferred calibration. However, the complicated conditions for the calibration transfer likely contributed to these large differences in AOD. On the other hand, the fact that the discrepancies between the calculated and the reference AOD are similar in both analyses may indicate that the differences introduced by the UILP calibration are of the same order as those associated with the CIMEL-transferred calibration.

Concerning traceability, represented by the percentage of data points within the WMO limits (Table 3.2.4), more than 90% of the AOD differences lie within these limits at every wavelength (see also Figures 3.2.5c and 3.2.5d). This good agreement is also shown in Figure 3.2.6, where the AOD differences are plotted over time together with the WMO limits.

Table 3.2.4 Statistical parameters of the AOD differences between Sunrad (applied to UVEG Prede data with UILP calibration) and AERONET ($\Delta AOD = AOD_{Sunrad} - AOD_{AERONET}$) at the available channels: Root Mean Square Error (RMSE), Standard Deviation of the differences (DIFF STD), Mean Bias Deviation (MBD), 90th percentile (P90), correlation coefficient R^2 and percentage of differences within the WMO limits (% WMO).

	RMSE	DIFF STD	MBD	P90	R^2	% WMO
ΔAOD_{500}	0.0037	0.0020	-0.0028	0.0008	0.9176	98.0
ΔAOD_{675}	0.0016	0.0011	0.0004	0.0024	0.9025	100
ΔAOD_{870}	0.0030	0.0016	-0.0020	0.0016	0.4890	99.7
ΔAOD_{1020}	0.0038	0.0022	0.0010	0.0058	0.4442	94.2

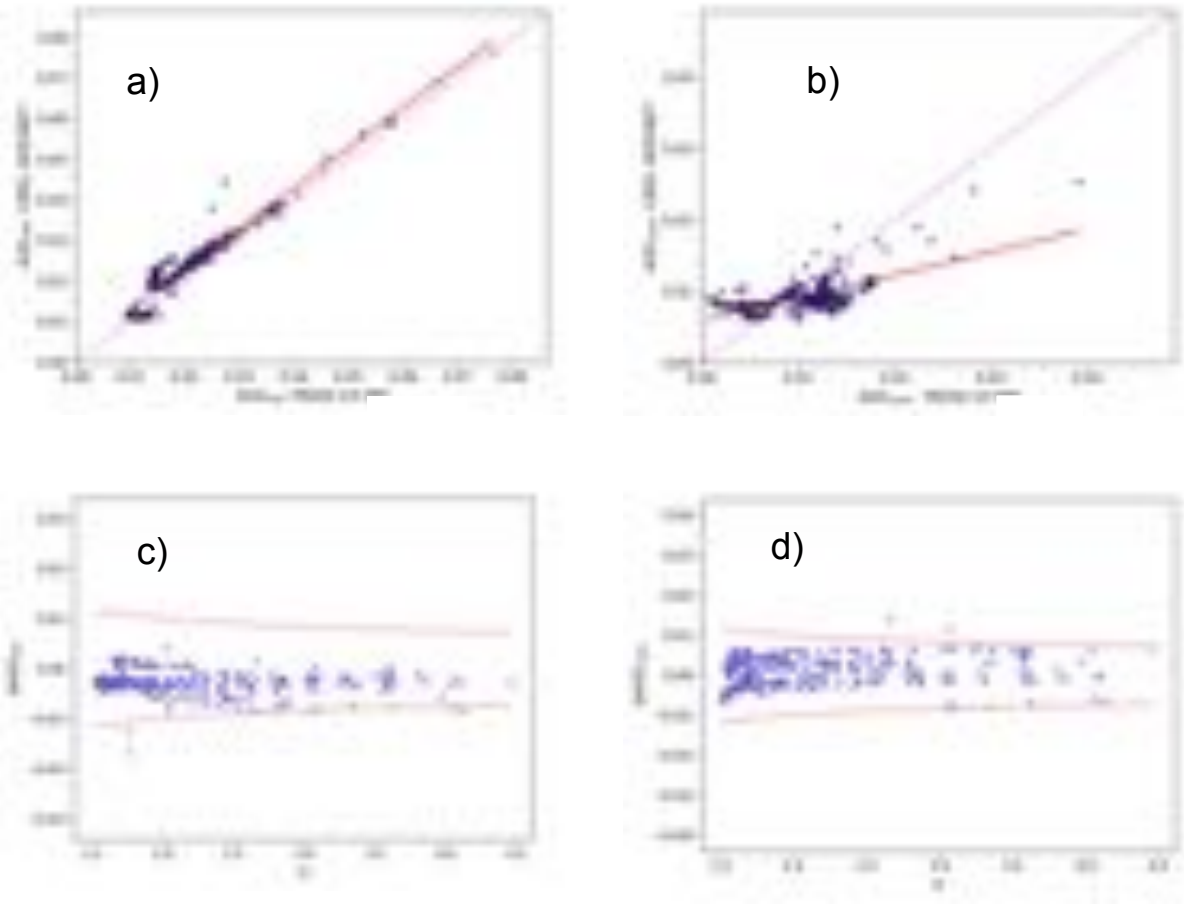


Figure 3.2.5 Scatter plots of AOD at 500 nm (a) and 1020 nm (b) obtained by AERONET (y-axis) and by Sunrad applied to UVEG Prede data with UILP calibration (x-axis). The pink dashed line has slope 1 and represents perfect agreement, while the red line shows the linear regression of the data points. In a), the regression line is $AOD_{AERONET} = 0.998\, AOD_{SUNRAD} + 0.003$, while in b) it is $AOD_{AERONET} = 0.322\, AOD_{SUNRAD} + 0.006$. Figures c) and d) show the AOD differences as a function of the air mass at 500 and 1020 nm, respectively. The red curves indicate the WMO limits for the traceability of the instruments.

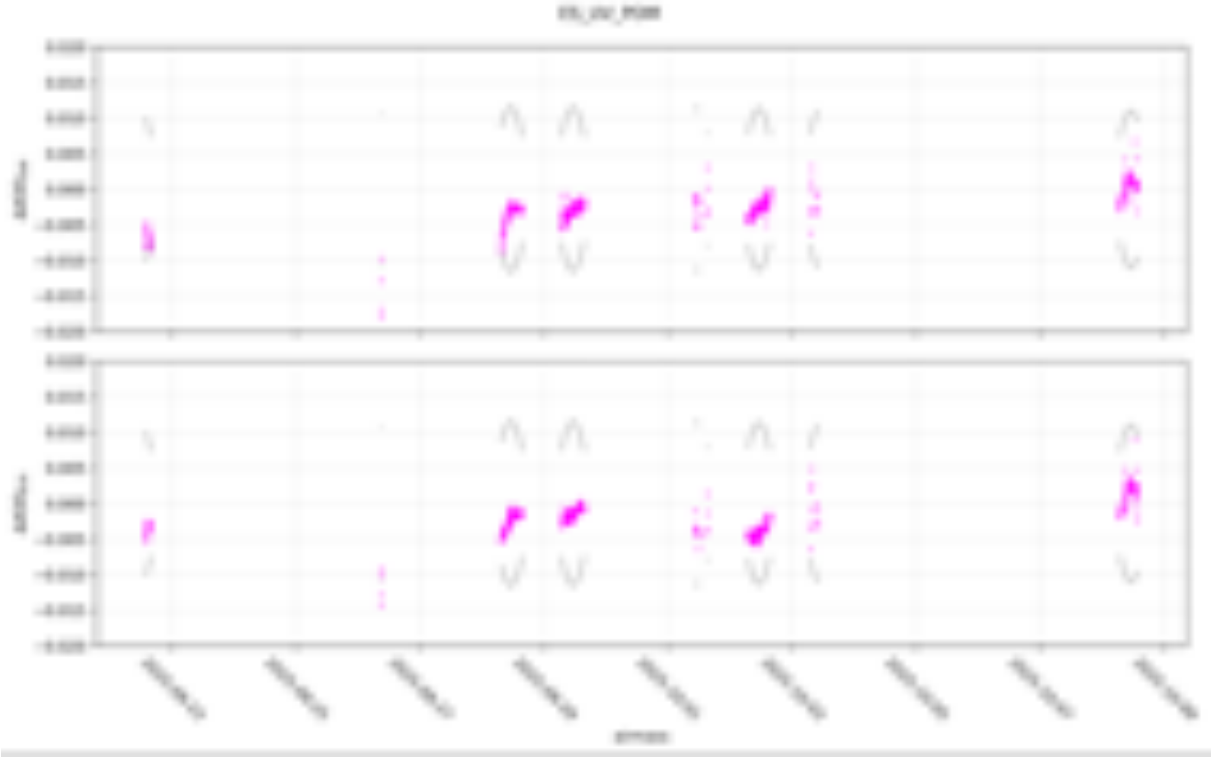


Figure 3.2.6 Evolution over time of the AOD differences between Sunrad (applied to UVEG Prede data) and AERONET (applied to CIMEL #1144), together with the WMO limits, at 500 nm (upper) and 870 nm (lower).

- CNR Prede (from CNR/ISAC, Rome):

Measurements collected by the CNR Prede from 22 September to 17 October have also been processed with Sunrad ISDC. For the computation, the default *meteo.dat* file was used, and the pre- and the post-campaign calibration coefficients determined using the UILP method were applied. The scatter plots of the Sunrad and AERONET computed AOD are shown in Figures 3.2.7a and 3.2.7b. As in the previous analysis, we studied how many of these differences fell within the WMO limits (Figures 3.2.7c, 3.2.7d and 3.2.8), as well as the statistical parameters characterising these AOD differences (Table 3.2.5). Compared with the UVEG Prede results, the discrepancies between the AOD obtained from the CNR Prede and AERONET are slightly higher. Furthermore, the R^2 values at 870 and 1020 nm are even lower than for the UVEG Prede. Despite this, the percentage of AOD differences within the WMO limits is higher than 80% at all the wavelengths, and exceeds 90% at 675 and 870 nm (see also Figure 3.2.8).

Table 3.2.5 Statistical parameters of the AOD differences between Sunrad (applied to CNR Prede data with UILP calibration) and AERONET ($\Delta AOD = AOD_{Sunrad} - AOD_{AERONET}$) at the

available channels: Root Mean Square Error (RMSE), Standard Deviation of the differences (DIFF STD), Mean Bias Deviation (MBD), 90th percentile (P90), correlation coefficient R^2 and percentage of differences within the WMO limits (% WMO).

	RMSE	DIFF STD	MBD	P90	R^2	% WMO
ΔAOD_{340}	0.0069	0.0039	0.0009	0.0091	0.8537	82.1
ΔAOD_{500}	0.0070	0.0034	-0.0042	0.0041	0.7010	85.6
ΔAOD_{675}	0.0051	0.0033	-0.0004	0.0062	0.4202	96.4
ΔAOD_{870}	0.0047	0.0027	-0.0005	0.0067	0.1617	93.6
ΔAOD_{1020}	0.0036	0.0022	-0.0008	0.0038	0.2858	89.3

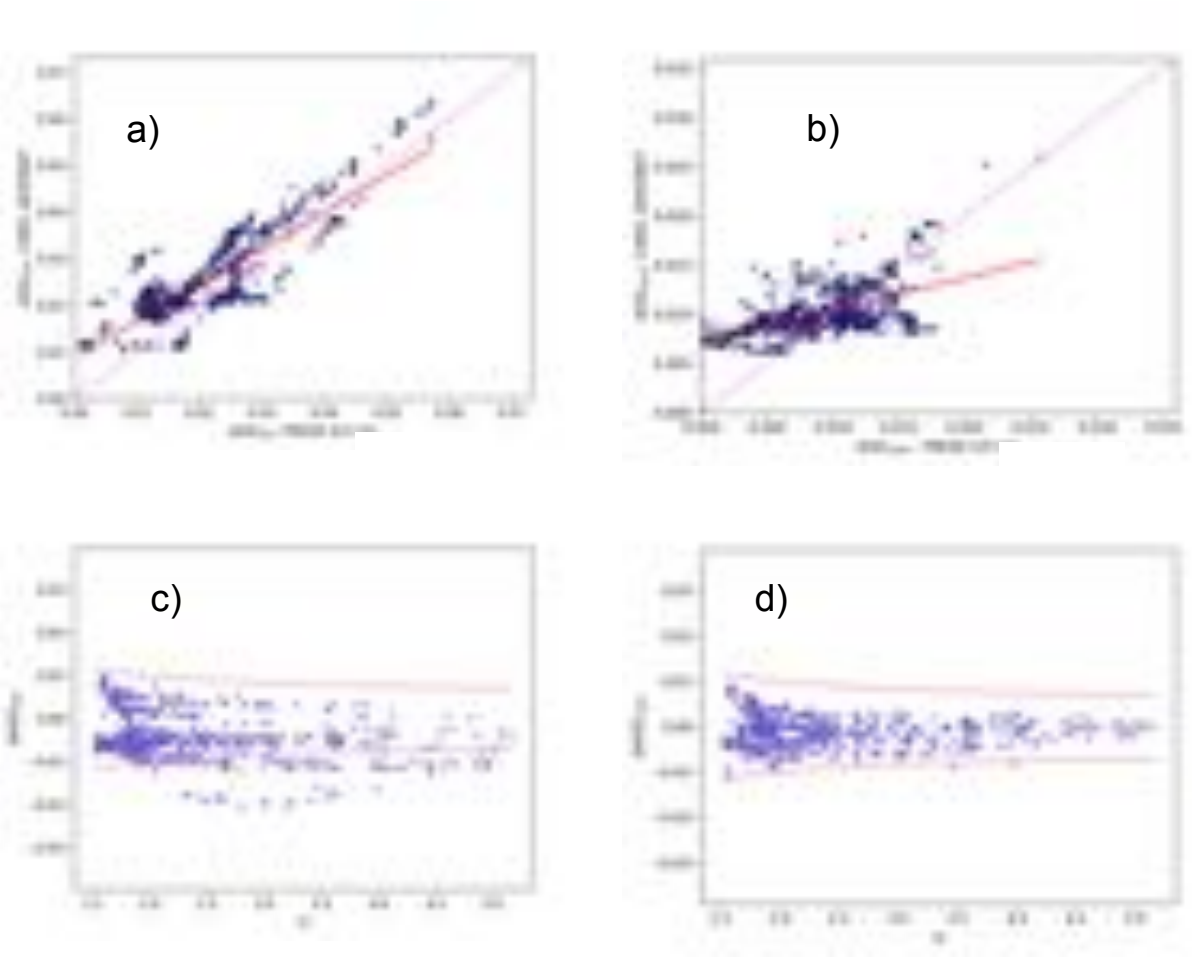


Figure 3.2.7 Scatter plots of AOD at 500 nm (a) and 1020 nm (b) obtained by AERONET (y-axis) and by Sunrad applied to CNR Prede data with UILP calibration (x-axis). The pink dashed line has slope 1 and represents perfect agreement, while the red line shows the linear regression of the data points. In a), the regression line is $AOD_{AERONET} = 0.783\ AOD_{SUNRAD} + 0.009$, while in b) it is $AOD_{AERONET} = 0.331\ AOD_{SUNRAD} + 0.007$. Figures c) and d) show the AOD differences as a function of the air mass at 500 and 1020 nm, respectively. The red curves indicate the WMO limits for the traceability of the instruments.

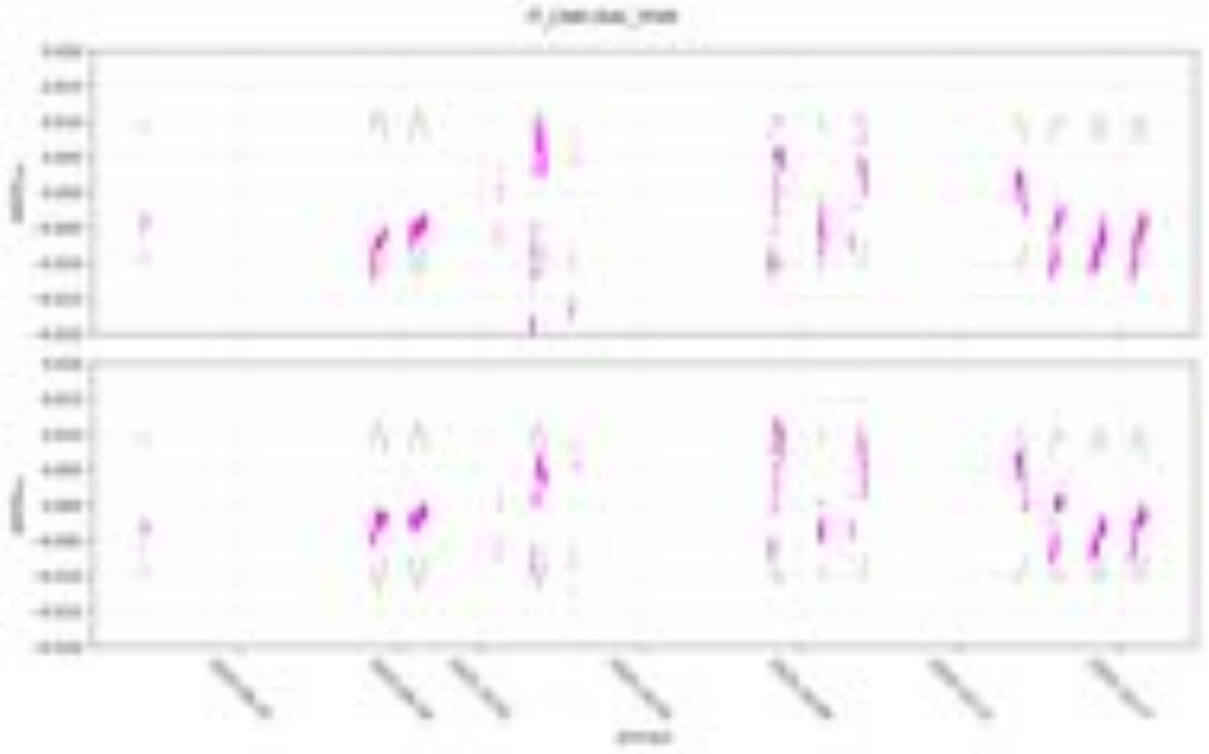


Figure 3.2.8 Evolution over time of the AOD differences between Sunrad (applied to CNR Prede data) and AERONET (applied to CIMEL #1144 data), together with the WMO limits, at 500 nm (upper) and 870 nm (lower).

3.2.5. Conclusions

In this study, we have used data collected during the FRC-VI campaign to examine the performance of the Sunrad algorithm in the retrieval of AOD under different configurations. AERONET's product for CIMEL #1144 is taken as the reference.

The first analysis consisted of processing the CIMEL #1144 raw data using Sunrad with the CIMEL's calibration, in order to study the effect of the algorithm on the calculation. Very good agreement is found between the obtained AOD and the AERONET retrievals, with an RMSE of ΔAOD smaller than 0.003 for every channel except 340 nm, for which the RMSE reaches 0.007. Nevertheless, in order to properly retrieve AOD_{1020}, it was crucial to take into account the temperature dependence of the calibration coefficients.

Then, the UVEG Prede data were processed with Sunrad, using as calibration the coefficients transferred from CIMEL #1144. Hence, in this case, both the algorithm and the instrumentation differ from AERONET's AOD retrieval for the CIMEL. However, the calibration transfer proved quite challenging as a result of the limited number of coincident measurements, due to cloudy days and the temporal mismatch between the instruments. Because of this, larger discrepancies than expected were found in the comparison of the obtained AOD.

Finally, the effect of calibration on the retrieval has been taken into account by processing the UVEG and CNR Prede data with Sunrad, using the corresponding calibrations obtained with the UILP method. Due to the problems experienced by the UVEG Prede from 9 October onwards, only the pre-campaign calibration was applied in this case. The differences between the AOD derived from Sunrad and that from AERONET are of a similar magnitude to the discrepancies observed in the previous analysis. In the case of the CNR Prede data, processed by Sunrad using both pre- and post-campaign calibrations, good agreement was also observed with the AERONET AOD for CIMEL #1144, although the comparison was slightly less satisfactory than for the UVEG. In all cases, more than 90% of the AOD differences remained within the WMO limits, except at 340, 500 and 1020 nm for the CNR Prede (82-89%).

3.2.6. Outlook

The Sunrad algorithm allows the processing of direct irradiance data from Prede and CIMEL sun photometers with a unified method for calculating AOD, AE and TCWV. Therefore, it is important to continue efforts to improve this algorithm in order to homogenise retrievals from different instruments. Planned future work includes implementing the processing of the 1640 nm channel; improving the characterisation of atmospheric gases and of the temperature dependence of the calibration coefficients; and adapting the PFR file format so that it can be processed by this algorithm. The extensive dataset from the Prede, CIMEL and PFR instruments installed at the same location in Lindenberg is expected to be used for the development of this algorithm.

4. Harmonisation for lunar photometry: Moonrad (SKYNET algorithm for lunar photometry)

Lunar AOD measurements based on lunar irradiance have been successfully implemented using Lunar ground-based radiometers in AERONET (Barreto et al., 2013; 2017) and PFR (Mazzola et

al., 2024). These developments successfully demonstrated the potential of extending the measurements during the nighttime, reducing the data gap. Within SKYNET, Moonrad was developed for nighttime aerosol products using lunar irradiance measurements performed with the lunar Prede POM 1/2 radiometers.

4.1. Moonrad implementation and structure

4.1.1 Moonrad

Moonrad is based on the Sunrad algorithm (Estellés et al., 2012), which is used to retrieve the aerosol optical properties using the direct Sun data during daytime. Figure 4.1.1 presents the workflow of Moonrad. As illustrated in the Figure, it consists of three modules, namely ROLO, DSFORM and DSPROC.

4.1.2. ROLO module

The processing starts by feeding date, time, and location to the ROLO module. ROLO (Robotic Lunar Observatory: lunar reflectance model of USGS, Kieffer and Stone (2005)) provides the lunar reflectance. SPICE library is then used to calculate the required Sun-Moon-Earth geometrical parameters, including the selenographic coordinates and lunar phase angle. This information is then used to calculate the lunar disk-equivalent reflectance using the ROLO model. However, ROLO provides the disk-equivalent reflectance at 32 discrete wavelengths spanning 350-2383 nm. Therefore, the modelled reflectance is interpolated to the standard wavelengths of Prede POM channels (380, 400, 500, 675, 870 and 1020 nm). Since the 340 nm channel lies outside the wavelength range covered by ROLO, the corresponding disk-equivalent reflectance at 340 nm is extrapolated.

4.1.3. DSFORM and DSPROC

The ROLO reflectance and raw lunar irradiance data are then simultaneously sent to the DSFORM module, where every minute data of ROLO reflectance is interpolated to the exact timestamps of the raw lunar irradiance observations. The time-matched ROLO reflectance is then combined with the raw lunar irradiance measurements to correct for the non-uniform reflectance of the lunar disk. The corrected data is then formatted to generate a set of 1 minute data.

The formatted data generated by the DSFORM module is sent to the DSPROC module, where nighttime AOD is retrieved using Beer's law. The AOD retrieval starts by calculating the lunar calibration values using the method proposed by Uchiyama et al. (2019).

The minutely files generated by DSFORM are subsequently passed to the DSPROC module, where nighttime AOD is retrieved. In this step, the lunar signal is processed using calibration coefficients determined following the methodology described by Uchiyama et al. (2019). The calibration values are then used to calculate the total optical depth, from which the contributions of Rayleigh scattering and gaseous absorption are removed to obtain the nighttime AOD. Finally, cloud screening removes cloud-contaminated data. The gas correction and cloud-screening procedures used in this module use the same methodology implemented in Sunrad.

As shown at the bottom of Figure 4.1.1, Moonrad produces two levels of data: Level 2A and Level 2. Level 2A data is produced using the calibration values available at the time of processing, whereas Level 2 data is generated after reprocessing using both pre- and post-calibration.

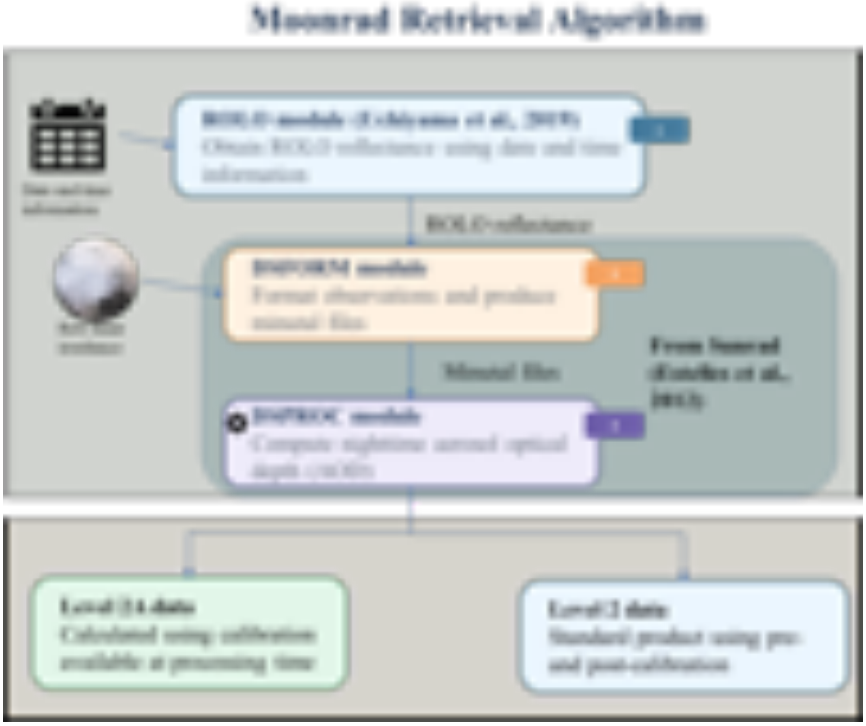


Figure 4.1.1 Workflow of the Moonrad Processing.

4.2. Comparison to CIMEL lunar AOD

4.2.1. Dataset

In this study, we used the data from the QUATRAM III campaign in Rome, Italy, and the Izaña campaign on the island of Tenerife, Spain. The campaigns were conducted from 1-20 September 2021 and 2-22 September 2022, respectively. During both campaigns, we obtained nighttime lunar irradiance measurements using the Lunar Prede POM-01 operated by CNR/ISAC. For intercomparison and validation, we used the corresponding AERONET version 3 level 2 nighttime direct AOD products as a reference.

4.2.2. Intercomparison with AERONET

To assess Moonrad performance, we compared the nighttime AOD retrieved with Moonrad with the corresponding AERONET version 3 level 2 data during the QUATRAM III and Izaña campaigns. For the comparative analysis, we selected simultaneous data within a 10-second temporal gap. The comparison was evaluated using correlation analysis, including the correlation coefficient and RMSD. Additionally, we evaluated AOD differences by creating a WMO plot and counting points within the WMO limit, defined as ± (0.005 + 0.01/m), where m is the airmass.

The correlation plots in Figures 4.2.1 and 4.2.2 show that the Prede agrees very well with the corresponding AERONET nighttime AOD during QUATRAM III and Izaña campaigns, with all the measurements lying close to the 1:1 line. This strong agreement is also supported by statistics shown in Table 4.2.1, where the correlation coefficient (r) ranges from 0.97 to 0.99, indicating an almost linear relationship between the two datasets during both campaigns. Additionally, the magnitude of RMSD remains below 0.009 for all the wavelengths during both campaigns, further demonstrating a very good consistency between the Prede and CIMEL (AERONET) nighttime AOD measurements.

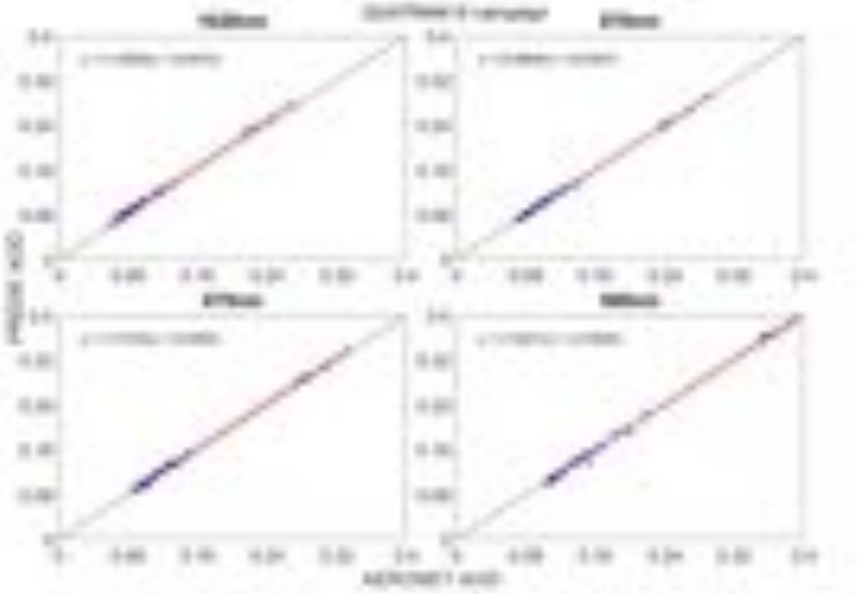


Figure 4.2.1 Correlation plot of AERONET and Moonrad nighttime AOD in QUATRAM III.

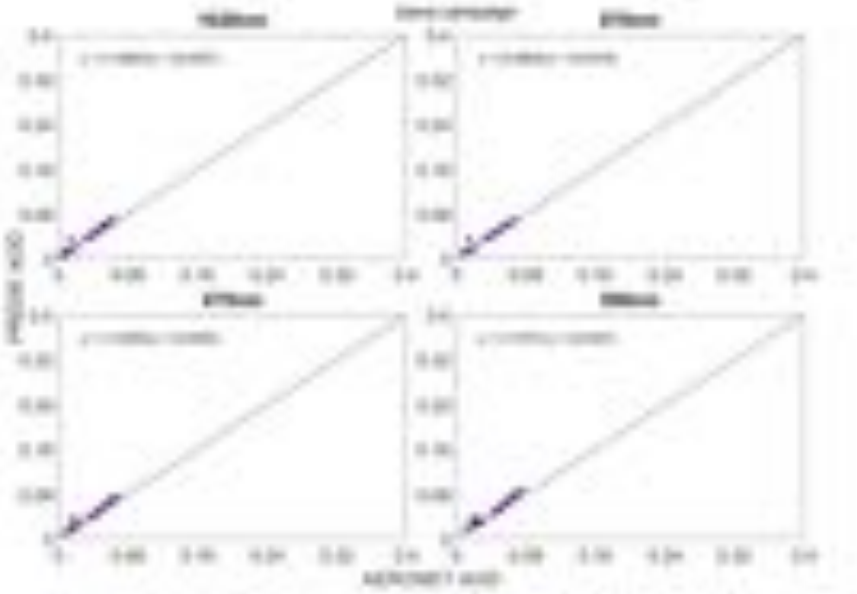


Figure 4.2.2 Correlation plot of AERONET and Moonrad nighttime AOD in Izaña campaign.

Table 4.2.1 RMSD and correlation coefficient (r) of Moonrad and AERONET nighttime AOD during QUATRAM III and MAPP campaigns.

Campaign	500 nm	675 nm	870 nm	1020 nm		No of point
QUATRAM III	0.0045	0.0039	0.0023	0.0064	RMSD	40
	0.99	0.99	0.99	0.99	r	
Izaña	0.0083	0.0067	0.0047	0.0063	RMSD	46
	0.98	0.98	0.97	0.98	r	

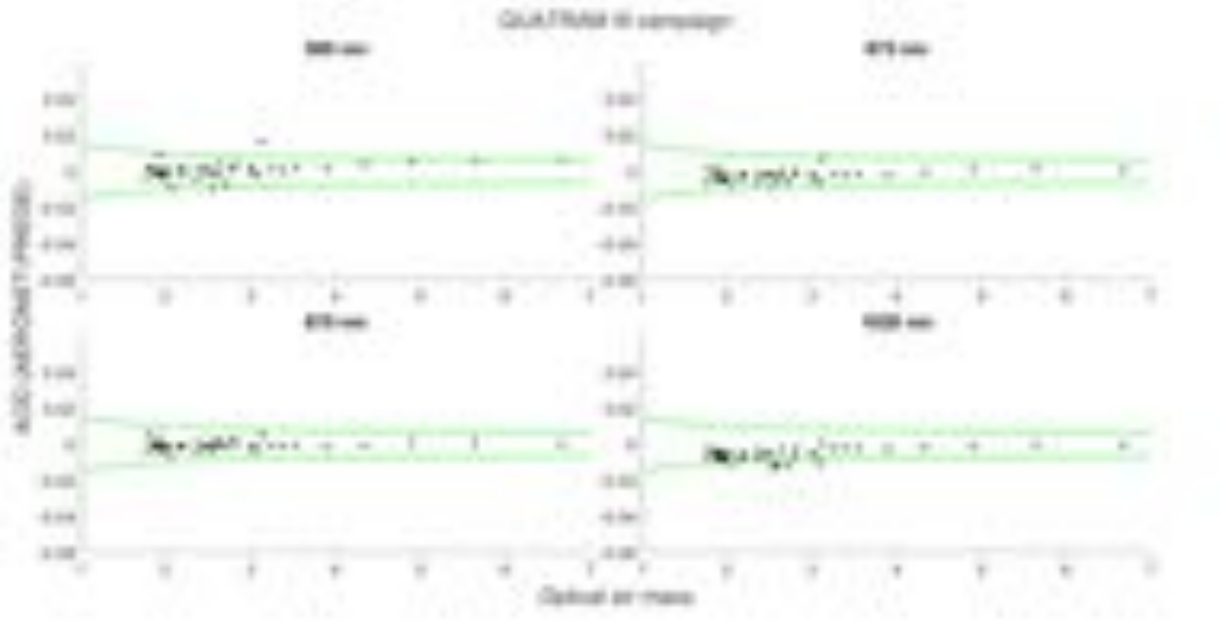


Figure 4.2.3 Distribution of the nighttime AOD data within the WMO limit (green lines) in the QUATRAM III campaign.

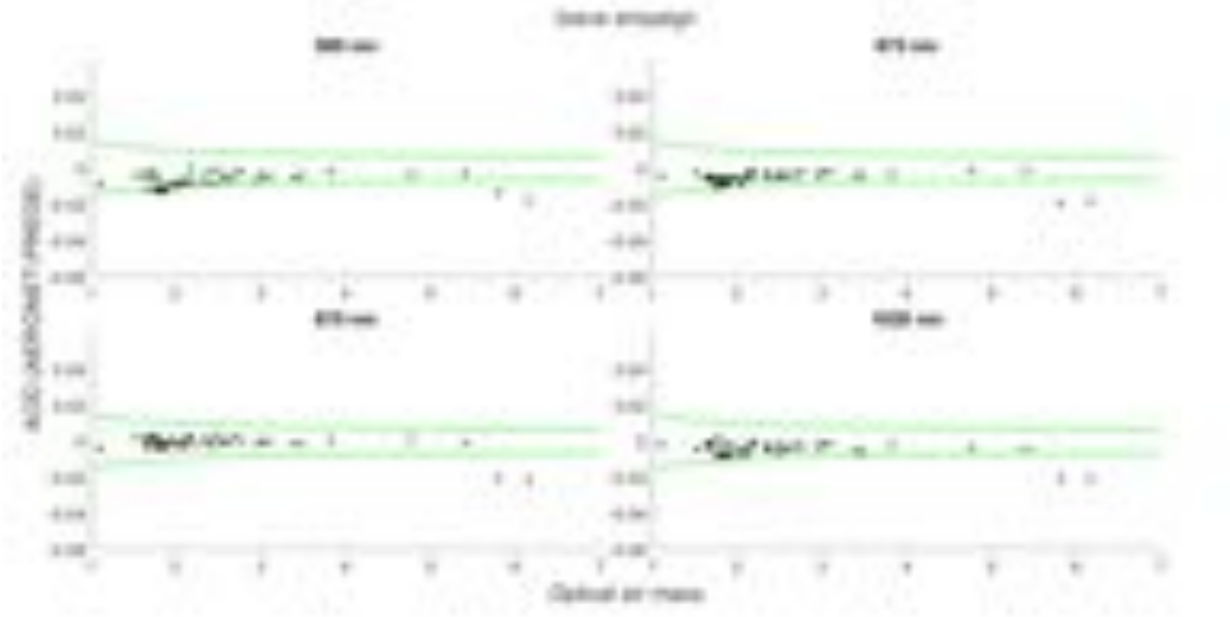


Figure 4.2.4 Distribution of the nighttime AOD data within the WMO limit (green lines) in the Izaña campaign.

Table 4.2.2 Percentage of points following the WMO limit in QUATRAM III and MAPP campaigns.

	500 nm	675 nm	870 nm	1020 nm	Campaigns
Data within WMO limit (%)	95	97.5	100	85	QUATRAM III
	73.91	93.48	95.65	95.65	MAPP

The WMO comparison is presented in Figures 4.2.3, 4.2.4 and Table 4.2.2. These results show that the majority of the data within the WMO limit (within green lines) satisfy the WMO acceptance criteria (Kazadzis et. al., 2018b). The fraction of points within the WMO limits varies from 85 to 100% and from 73.91 to 95.65% across all wavelengths during the QUATRAM III and Izaña campaigns. The comparatively low fraction of points at 1020 nm during the QUATRAM III campaign (85%) and 500 nm during the Izaña campaign (73.9%) may be due to limited data available for the analysis. With only 40 and 46 simultaneous measurements available for the analysis, only a few points going outside the WMO limit can cause a noticeable reduction in the percentage of points within the WMO acceptance criteria. Overall, WMO statistics also indicate good agreement between the two datasets, and further support the consistency between the nighttime AOD retrieved using the Moonrad from Prede lunar measurements and the AERONET nighttime AOD product.

4.2.3. Future work

The present results demonstrate the reliability of Moonrad in retrieving nighttime AOD in the QUATRAM III and Izaña campaigns. In future, Moonrad should be evaluated at more stations covering a broader range of atmospheric conditions and aerosol loading.

5. Summary

This deliverable demonstrates how COST Action HARMONIA achieved its main goal: harmonising methods and techniques for aerosol remote sensing, particularly the measurement and retrieval of aerosol optical depth (AOD), and reducing differences between the approaches used by the networks that provide the data: AERONET for CIMEL instruments, SKYNET for Prede instruments, and GAW-PFR for PFR instruments.

Part 2 of the deliverable focuses on the studies and efforts devoted to comparing AOD using a common equation (Equation E2.8 in Section 2.1) and common atmospheric-component amounts as inputs to the retrieval procedure. The resulting harmonised AOD, denoted (AOD_{harm}), is instrument-specific—because each instrument makes its own raw radiometric measurements—but no longer network-specific. The greatest advantage of working with the harmonised AOD, is that comparing (AOD_{harm}) values from different instruments makes it possible to investigate the influence of calibration methods and the instruments themselves. The pure effect on AOD of post processing differences between AERONET and GAW-PFR was typically below 0.005 although on a few occasions approached 0.01. The harmonisation process sometimes improves the AOD agreement between the instruments, sometimes makes it worse. More often it leads to improvements (the AOD differences are usually smaller for the harmonised dataset (AOD_{harm}) than for the original dataset (AOD_{netw})). Section 2.2 presents comparisons of Prede, PFR, and CIMEL instruments using the Lindenberg AOD dataset, while Section 2.3 examines how measurement-site characteristics affect CIMEL–PFR comparisons at Davos, Hohenpeißenberg, Izaña, and Valladolid. AOD comparison studies were previously presented in HARMONIA Deliverable D1.2 (Doppler et al., 2024). However, over the two years since then, the collaborative work enabled and supported by COST Action HARMONIA—bringing together researchers working with the different networks—has made it possible to present in Deliverable D1.3 the results and benefits of these harmonisation efforts.

Part 3 of the deliverable presents activities from the latest major AOD comparison campaign organised every five years by the WMO: the Filter Radiometer Comparison (FRC). This section continues the work presented in an earlier HARMONIA deliverable. Deliverable D1.1 (Doppler et al., 2023) described major campaigns on aerosol remote sensing and AOD measurements that took place before or at the beginning of COST Action HARMONIA. The sixth Filter Radiometer Comparison (FRC-VI), held in September and October 2025, was not covered in that deliverable. Many HARMONIA participants took part in FRC-VI with their instruments. The campaign is described in Section 3.1. This deliverable focuses on the harmonisation efforts undertaken during COST Action HARMONIA. Accordingly, Section 3.2 presents two harmonisation experiments conducted in Davos during FRC-VI and supported by a HARMONIA Short-Term Scientific Mission

(STSM) grant. The experiments assessed differences between the AERONET and SKYNET networks using SKYNET's Sunrad algorithm. First, the Sunrad AOD retrieval algorithm was applied to raw measurements from an AERONET CIMEL instrument. The resulting AOD values were compared with AERONET AOD products and showed convincing agreement. Second, the calibration of a CIMEL instrument—performed at an AERONET calibration centre using the AERONET calibration procedure—was transferred to a SKYNET Prede instrument. AOD retrieved from the calibrated Prede measurements using Sunrad was then compared with the AERONET AOD product from the CIMEL instrument at Davos. The comparison was very satisfactory for one instrument at some wavelengths. For another instrument and other wavelengths, the differences revealed important insights into the conditions required for successful calibration transfer.

Part 4 of the deliverable presents the extension of SKYNET AOD measurements and retrievals from sun photometry to lunar photometry. The SKYNET Moonrad algorithm has been implemented to retrieve AOD from raw lunar radiation measurements made by Prede instruments. Its implementation was guided by efforts to harmonise it with AERONET methods and drew on lessons from ten years of AERONET lunar photometry across several hundred stations. Finally, the AOD values retrieved using Moonrad are compared with AERONET lunar AOD measurements. The good agreement between the two datasets provides validation for Moonrad.

All the studies presented here would not have been possible without the collaborative environment fostered by COST Action HARMONIA. It brought together people from different measurement networks, professional roles, and institutions—including academic research organisations, government agencies, and instrument manufacturers—to conduct joint research projects supported by HARMONIA grants for virtual mobility (VM) and Short-Term Scientific Missions. The knowledge gained is substantial, even if it cannot be quantified. The studies presented here provide an overview of this work. Although COST Action HARMONIA has now concluded, the community remains active and will continue to collaborate, further develop these studies, and pursue new research in this field. As a short-term legacy, the COST Action HARMONIA inter-journal special issue in Atmospheric Measurement Techniques and Atmospheric Chemistry and Physics (EGU edition), "Sun-photometric measurements of aerosols: harmonization, comparisons, synergies, effects, and applications" will remain open for the next two years. The results of the studies presented in this deliverable, along with those of the outlook studies mentioned here, will soon be published in this special issue. We look forward to seeing you there: https://amt.copernicus.org/articles/special_issue1356.html

References

1. Barreto, A., Cuevas, E., Damiri, B., Guirado, C., Berkoff, T., Berjón, A. J., Hernández, Y., Almansa, F., and Gil, M.: A new method for nocturnal aerosol measurements with a lunar photometer prototype, Atmos. Meas. Tech., 6, 585–598, https://doi.org/10.5194/amt-6-585-2013, 2013.

2. Barreto, Á., Román, R., Cuevas, E., Berjón, A. J., Almansa, A. F., Toledano, C., González, R., Hernández, Y., Blarel, L., Goloub, P., Guirado, C., and Yela, M.: Assessment of nocturnal aerosol optical depth from lunar photometry at the Izaña high mountain observatory, Atmos. Meas. Tech., 10, 3007–3019, https://doi.org/10.5194/amt-10-3007-2017, 2017.
3. Bodhaine, B. A., Wood, N. B., Dutton, E. G. and Slusser, J. R.: On Rayleigh Optical Depth Calculations, Journal of Atmospheric and Oceanic Technology, Vol 16. Issue 11, https://doi.org/10.1175/1520-0426(1999)016<1854:ORODC>2.0.CO;2, 1999.
4. Doppler, L., Masoom, A., and Karanikolas, A.: COST-HARMONIA WG1, Deliverable D1.1: Create a list of existing and foreseen campaigns or experiments needed for night and day aerosol measurements and report on the data collection and analysis of the data/measurements, https://harmonia-cost.eu/wp-content/uploads/2023/10/COST_CA21119_HARMONIA-WG1_Deliverable-D11.pdf, 2023.
5. Doppler, L., Akriti Masoom, et al.: COST-HARMONIA WG1, Deliverable D1.2: Differences and harmonisation possibilities in AOD retrieval methods, https://harmonia-cost.eu/wp-content/uploads/2024/12/Harmonia_D1.2_ver2.pdf, 2024.
6. Estellés, V., Campanelli, M., Smyth, et al.: A.: Evaluation of the new ESR network software for the retrieval of direct sun products from CIMEL CE318 and PREDE POM01 sun-sky radiometers, Atmos. Chem. Phys., 12, 11619–11630, https://doi.org/10.5194/acp-12-11619-2012, 2012.
7. Fröhlich, C. and Shaw, G.E.: New determination of Rayleigh scattering in the terrestrial atmosphere. Applied Optics, 19(11), pp.1773-1775., https://doi.org/10.1364/AO.19.001773, 1980.
8. Giles, D. M., Sinyuk, A., Sorokin, M. G., et al.: Advancements in the Aerosol Robotic Network (AERONET) Version 3 database – automated near-real-time quality control algorithm with improved cloud screening for Sun photometer aerosol optical depth (AOD) measurements, Atmos. Meas. Tech., 12, 169–209, https://doi.org/10.5194/amt-12-169-2019, 2019.

9. González, R., Toledano, C., Román, R., et al.: Daytime and nighttime aerosol optical depth implementation in CÆLIS, Geosci. Instrum. Method. Data Syst., 9, 417–433, https://doi.org/10.5194/gi-9-417-2020, 2020.
10. Group of Atmospheric Optics, Valladolid University. (n.d.). CÆLIS [Software]. CÆLIS. Last seen: October 1, 2026, from https://www.caelis.uva.es/aboutus
11. Gueymard, C., SMARTS2 A simple model of atmospheric radiative transfer of sunshine, Report FSEC-PF-270-95, Florida Solar Energy Center, https://ww.instesre.org/GCCE/SMARTS2.pdf, 1995.
12. Karanikolas, A., Kouremeti, N., Gröbner, J., Egli, L., and Kazadzis, S.: Sensitivity of aerosol optical depth trends using long-term measurements of different sun photometers, Atmos. Meas. Tech., 15, 5667–5680, https://doi.org/10.5194/amt-15-5667-2022, 2022.
13. Karanikolas, A., Kouremeti, N., Campanelli, M., Estellés, V., Momoi, M., Kumar, G., Nyeki, S., and Kazadzis, S.: Intercomparison of aerosol optical depth retrievals from GAW-PFR and SKYNET sun photometer networks and the effect of calibration, Atmos. Meas. Tech., 17, 6085–6105, https://doi.org/10.5194/amt-17-6085-2024, 2024.
14. Karanikolas, A., Torres, B., Momoi, M., Herreras-Giralda, M., Kouremeti, N., Gröbner, J., Doppler, L., and Kazadzis, S.: Retrieval of Aerosol Properties from Direct Solar Irradiance Measurements with High Temporal Resolution and Spectral Range, Atmos. Meas. Tech., 18, 7651–7677, https://doi.org/10.5194/amt-18-7651-2025, 2025.
15. Karanikolas, A., Doppler, L., Hrabcák, P., and Anyfanti, K.:COST-HARMONIA WG1, Deliverable D1.4: Spectral AOD and AOD in the UV, COST ACTION, COST-EUROPEAN COOPERATION IN SCIENCE AND TECHNOLOGY, Brussels, Belgium, COST CA21119 HARMONIA-WG1 Deliverable-D1.4, https://harmonia-cost.eu/wp-content/uploads/2026/10/WG1-D1.4-Spectral-and-UV-AODHARMONIAtemplate.pdf, 2026.
16. Kazadzis, S., Kouremeti, N., Nyeki, S., Gröbner, J., and Wehrli, C.: The World Optical Depth Research and Calibration Center (WORCC) quality assurance and quality control of GAW-PFR AOD measurements, Geosci. Instrum. Method. Data Syst., 7, 39–53, https://doi.org/10.5194/gi-7-39-2018, 2018a.

17. Kazadzis, S., Kouremeti, N., Diémoz, H., et al.: Results from the Fourth WMO Filter Radiometer Comparison for aerosol optical depth measurements, Atmos. Chem. Phys., 18, 3185–3201, https://doi.org/10.5194/acp-18-3185-2018, 2018b.
18. Kazadzis, S., Kouremeti, N., and Gröbner, J.: Fifth WMO Filter Radiometer Comparison (FRC-V) 27 September to 25 October 2021, Davos, Switzerland, WMO GAW report 280, https://library.wmo.int/records/item/66263-fifth-wmo-filter-radiometer-comparison-frc-v?offset=5 (last access: 1 February 2024), 2023.
19. Kazadzis, S., Estellés, V., G. Campanelli, M. and Scarlatti F.: Report on the links of metrology MAPP project results and measurement accuracy and uncertainty improvements and an example of machine learning techniques towards the retrieval of aerosol properties, COST ACTION, COST-EUROPEAN COOPERATION IN SCIENCE AND TECHNOLOGY, Brussels, Belgium, https://harmonia-cost.eu/wp-content/uploads/2024/11/Harmonia_D23_f.pdf (last access: 13 April 2026), 2024.
20. Kasten, F.: A new table and approximation formula for the relative optical air mass. Arch. Met. Geoph. Biokl. B. 14, 206–223. https://doi.org/10.1007/BF02248840, 1966.
21. Kasten, F. and Young, A.T.: Revised optical air mass tables and approximation formula, Applied Optics, 28, 4735- 4738, https://doi.org/10.1364/AO.28.004735, 1989.
22. Kieffer, H. H. and Stone, T. C.: The spectral irradiance of the moon, Astron. J., 129, 2887–2901, https://iopscience.iop.org/article/10.1086/430185/pdf, 2005.
23. W. D. Komhyr, Dobson operations handbook, NOAA/CMDL, http://www.cmdl.noaa.gov/ozwv/dobson/papers/report6/report6.html, 1980.
24. Kumar, G., Momoi, M., Campanelli, M., et al.: Optimization of the SKYNET calibration with an iterative Improved Langley method and its validation in the Mediterranean area, EGUsphere [preprint], https://doi.org/10.5194/egusphere-2026-4267, 2026.
25. Mazzola, M., Stone, R. S., Kouremeti, et al.: Monitoring aerosol optical depth during the Arctic night: Instrument development and first results. *Atmospheric Research*, *311*, 107667. https://doi.org/10.1016/j.atmosres.2024.107667, 2024

26. Nakajima, T., Campanelli, M., Che, H., Estellés, et al..: An overview of and issues with sky radiometer technology and SKYNET, Atmos. Meas. Tech., 13, 4195–4218, https://doi.org/10.5194/amt-13-4195-2020, 2020.
27. Sinyuk, A., B. N. Holben, A. Smirnov, T. F. Eck, I. Slutsker, J. S. Schafer, D. M. Giles, and M. Sorokin (2012), Assessment of error in aerosol optical depth measured by AERONET due to aerosol forward scattering, Geophys. Res. Lett., 39, L23806, doi:10.1029/2012GL053894.
28. Sinyuk, A., Holben, B. N., Eck, T. F., Giles, D. M., Slutsker, I., Korkin, S., Schafer, J. S., Smirnov, A., Sorokin, M., and Lyapustin, A.: The AERONET Version 3 aerosol retrieval algorithm, associated uncertainties and comparisons to Version 2, Atmos. Meas. Tech., 13, 3375–3411, https://doi.org/10.5194/amt-13-3375-2020, 2020.
29. Uchiyama, A., Shiobara, M., Kobayashi, H., Matsunaga, T., Yamazaki, A., Inei, K., Kawai, K., and Watanabe, Y.: Nocturnal aerosol optical depth measurements with modified sky radiometer POM-02 using the moon as a light source, Atmos. Meas. Tech., 12, 6465–6488, https://doi.org/10.5194/amt-12-6465-2019, 2019.
30. WMO/TD-No. 1287. 2005, WMO/GAW Experts Workshop on a Global Surface-Based Network for Long Term Observations of Column Aerosol Optical Properties (8-10 March 2004), 2005
31. Wehrli, C.: Precision Filter Radiometer Documentation (PFR Manual V4.1), PMOD/WRC, 2009

Table of Acronyms

ACTRIS	Aerosol, Clouds and Trace Gases Research Infrastructure - Centre for Aerosol Remote Sensing
ACTRIS-CARS	ACTRIS - Centre for Aerosol Remote Sensing
AE	Ångström Exponent (α): characterize AOD spectral variation
AEMET	*Agencia Estatal de Meteorología* (meteorological service of Spain)
AERONET	AErosol RObotic NETwork: AOD and aerosol properties measurements network using CIMEL CE-318 photometer
AOD	Aerosol Optical Depth (also known as AOT: Aerosol Optical Thickness): Main parameter used to characterise aerosol amount and aerosol impact on radiation in the atmosphere. AOD is also the main parameter measured with photometers.
CÆLIS	Network and retrieval algorithm managed by GOA-UVa (Valladolid)
CARSNET	China Aerosol Remote Sensing Network
CNR	*Consiglio Nazionale delle Ricerche* (Italian national research council)

DU	Dobson Units
DWD	*Deutscher Wetterdienst* (German meteorological service)
EMPIR	European Metrology Programme for Innovation and Research
ESR	European SkyRad users' network
EURAMET	EURopean Association of national METrology institutes
FMI	Finnish Meteorological Institute, Finland (many places in Finland but the main place is in Helsinki).
FRC	WMO Filter Radiometer Comparisons organised on a 5-year schedule at PMOD/WRC in Davos, Switzerland. Together with the other WMO campaigns IPC and IPgC.
FRC-VI	Sixth WMO Filter Radiometer Comparison: WMO campaign organised in Davos at PMOD/WRC, September/October 2025
GAW	Global Atmosphere Watch: WMO Programme of trends monitoring of the atmosphere
GAW-PFR	Global Atmosphere Watch - Precision Filter Radiometer network: AOD measurement network of WMO/GAW Programme
GOA (GOA-UVa)	*Grupo de Óptica Atmosférica - Universidad de Valladolid* (Group of Atmospheric Optics)), Valladolid, Spain
HARMONIA	International network for harmonisation of atmospheric aerosol retrievals from ground-based photometers: Name of the COST action
IARC	Izaña Atmospheric Research Center (AEMET observatory at Izaña), Izaña, Tenerife, Spain
IPC	International Pyrheliometer Comparison (WMO campaign at PMOD/WRC, Davos)
IPCC	Intergovernmental Panel on Climate Change (WMO campaign at PMOD/WRC, Davos)
IPgC	International Pyrgeometer Comparison (WMO campaign at PMOD/WRC, Davos)
ISAC	*Istituto di Scienze dell'Atmosfera e del Clima*, CNR (Institute of Atmospheric Sciences and Climate), Rome, Italy
ISDC	International SKYNET Data Center
ISP	*Istituto di Scienze Polari*, CNR (Institute of polar science), Bologna, Italy
JMA	Japan Meteorological Agency
LOA	*Laboratoire d'Optique Atmosphérique* (Laboratory of ATmospheric Optics), University of Lille, France
MAPP	Metrology of Aerosol Optical Properties: EURAMET/EMPIR project campaign at Izaña (Tenerife, Spain), September 2022
MBAE	Mean Bias Absolute Error
MBD	Mean Bias Deviation
MBE	Mean Bias Error
MOHP	*Meteorologisches Observatorium Hohenpeißenberg, Deutscher Wetterdienst* (DWD observatory of Hohenpeißenberg), Hohenpeißenberg, Germany
MOL-RAO	*Meteorologisches Observatorium Lindenberg - Richard Aßmann Observatorium, Deutscher Wetterdienst* (DWD observatory of Lindenberg), Lindenberg (Tauche), Germany
PFR	Precision Filter Radiometer: Photometer manufactured by PMOD/WRC

PMOD/WRC	*Physikalisch-Meteorologisches Observatorium Davos* /World Radiation Center, Davos, Switzerland
POM	Precise design Of Meteorological and scientific instrument: Photometer manufactured by Prede and used in the network SKYNET.
RMSE	Root Mean Square Error
ROLO	Robotic Lunar Observatory: lunar reflectance model of USGS
SKYNET	SKY Measurements NETwork: AOD and aerosol properties measurements network using Prede-POM instrument
STSM	Short Term Scientific Mission: Grant possibility of a COST Action (including a visit to another institute)
SVA	Solid View Angle
TCWV	Total Column of Water Vapor (in mm of precipitable liquid water)
TOC	Total Ozone Column (in Dobson Units: DU)
TOD	Total Optical Depth
UILP	Updated Improve Langley Plot, see Kumar et al. 2026
USGS	United States Geological Survey, Flagstaff (AZ), USA
UVa	*Universidad de Valladolid* (University of Valladolid) Valladolid, Spain
UVEG	*Universitat de València Estudi General* (University of Valencia), Burjassot (Valencia), Spain
WG	Working Group
WMO	World Meteorological Organisation
WORCC	World Optical Depth Research Calibration Center (Calibration centre of GAW-PFR network, at at PMOD/WRC), Davos, Switzerland

Acknowledgements

The authors would like to thank Roberto Román Diez and Ramiro González Catón of the GOA-UVa group at the University of Valladolid (UVa) for their invaluable assistance with the study presented in section 2.2. They provided information about the processing of AERONET and CÆLIS products and, in particular, processed and reprocessed CÆLIS products for Lindenberg according to our specific requirements. We also thank Monica Campanelli (CNR/ISAC, Rome) and Víctor Estellés (UVEG, Valencia) for their assistance with section 2.2 and for providing information about the processing of the SKYNET dataset.
We would like to thank the technical staff of the DWD Lindenberg radiation group for keeping the AOD instrument suite in excellent operating condition over the years, which made the study of section 2.2 realisable.
We thank PMOD/WRC staff for their competence, their engagement and kindness by hosting all FRC (and IPC and IPgC) campaigns every five years in Davos, which made the studies of part 3 realisable.
Last but not least, we are grateful to the staff of GOA-UVa at the University of Valladolid and PHOTONS at LOA (Laboratoire d'Optique Atmosphérique), University of Lille, for calibrating our

CIMEL instruments for AERONET in Europe throughout the years. This service is provided free of charge and funded entirely by the calibration centres (LOA or GOA-UVa) and we extend our heartfelt thanks to them. This made the studies of part 2 and part 3 realisable.